SIMUATION AND EVALUATION OF OPTICAL TRANSPARENT CERAMIC SCINTILLATORS BASED HIGH-PERFORMANCE BRAIN PET SCANNER

A THESIS SUBMITTED TO THE GRADUATE SCHOOL OF APPLIED SCIENCES OF NEAR EAST UNIVERSITY

By
SAMUEL TADESSE ABEBE

In Partial Fulfillment of the Requirements for the Degree of Master of Science in Biomedical Engineering

NICOSIA, 2019

SAMUEL T. ABEBE SIMULATION AND EVALUATION OF OPTICAL TRANSPARENT CERAMIC SCINTILLATORS BASED HIGH-PERFORMANCE BRAIN PET SCANNER NEU 2019

SIMUATION AND EVALUATION OF OPTICAL TRANSPARENT SCINTILLATORS BASED HIGH-PERFORMANCE BRAIN PET SCANNER

A THESIS SUBMITTED TO THE GRADUATE SCHOOL OF APPLIED SCIENCES OF NEAR EAST UNIVERSITY

By
SAMUEL TADESSE ABEBE

In Partial Fulfillment of the Requirements for the Degree of Master of Science in Biomedical Engineering

NICOSIA, 2019

SAMUEL TADESSE ABEBE: SIMULATION AND EVALUATION OF OPTICAL TRANSPARENT CERAMIC SCINTILLATORS BASED HIGH-PERFORMANCE BRAIN PET SCANNER

Approval of Director of Graduate School of Applied Sciences

Prof. Nadir Cavus

We certify that this thesis is satisfactory for the award of the degree of Master of Science in Biomedical Engineering

Examining Committee in charge:

Prof. Dr. Ayşe Günay Kibarer	Head of the Department of Biomedical Engineering, NEU
Assoc. Prof. Dr. Dilber Uzun Özşahin	Supervisor, Department of Biomedical Engineering, NEU
Dr. Pavel Makarov	Co-supervisor, Innovation and communication Tech. Center, NEU
Asst. Prof. Dr. Boran Şekeroğlu	Information Systems Engineering, NEU
Assoc. Prof. Dr. Kamil Dimililer	Automotive Engineering, NEU

I hereby declare that all information in this document has been obtained and presented in accordance with academic rules and ethical conduct. I also declare that, as required by the rules and conduct, I have fully cited and referenced all material and results that are not original to this work.

Name, Last name: Samuel Tadesse, Abebe

Signature:

Date:

To my parents…

ACKNOWLEDGEMENT

First and for most “እግዚአብሔር ይመስገን” thanks GOD for the countless gifts you bestowed on me. My family, you have my life in such a positive way that words cannot express my appreciation. You are truly an inspiration.

I would like to express my deepest thanks and sincere appreciation to Assoc. Prof. Dr. Dilber Özşahin, Lecturer at biomedical engineering department, for her encouragement and comprehensive advices throughout my stay, and thank you for being part of my story, you are truly an inspiration.

I would like extend my appreciation and thanks to Dr. Pavel Makarov from Innovation and Information Technology Center for his ceaseless support and cooperation to finish my thesis work in the stipulated time.

It is a great pleasure to acknowledge my extreme deepest thanks and gratitude to Asst. Prof. Dr. İlker Özşahin, Lecture at biomedical engineering department, Near East University, for his advice, care and compassion throughout my stay. Again from the bottom of my heart, I thank you and appreciate all you have done.

Last but not least, I would like to thank Near East University for the scholarship, Ethiopian government for the sponsorship and my friends living here in Near East University and Ethiopia for their support and care.

ABSTRACT

In the last decennaries, brain PET imaging has become highly demanding for better diagnosis and disease pattern studies in brain cancer and mental disorders management. The performance of a PET system majorly described by its image spatial resolution, system sensitivity, and image quality where each one of them depends on their own factors optimized during the design and effectuation process. The purpose of this research is to design and simulate high-performance brain PET scanner employing cerium doped alkaline earth scintillating crystals introduced as optional class of detectors in the field. The system is designed and implemented using GATE and the performance is evaluated following NEMA NU4-2008 standard. The simulated scanner system has a cylindrical geometry with maximum and minimum inner radius of 320 mm and 280 mm, respectively. The cylinder is segmented into 58 heads and 1 x 1 x 10 mm^3 voxels with a total of 435,000 voxels with the scanner is simulated with three new materials, namely strontium hafnate (SHO), lutetium hafnate (LHO), and barium hafnate (BHO), and with lutetium Oxyorthosilicate (LSO) for comparison. The system performance with SHO, LHO, BHO, LSO has a quite close a mean spatial resolution measured axially at FWHM 1.13 mm, and 1.18, 1.10, 1.11, 1.12 for respective scintillators in mm, absolute sensitivity of 5.13%, 8.34%, 6.51%, 5.83% respectively, and the system has a scatter fraction of 13.2%, 13.19%, 13.19%, and 13.19% for SHO, LHO, BHO, LSO respectively and a mean scatter fraction of 13.2%. The results depicts that the suggested scintillators can be considered as promising detectors classes for high-performance brain PET imaging and other radiation detection applications.

***Keywords*:** PET; brain cancer; Scintillator; GATE

ÖZET

Son on yılda, beyin PET görüntüleme beyin kanseri ve zihinsel bozukluklar yönetiminde daha iyi tanı ve hastalık paterni çalışmaları için oldukça zorlayıcı hale geldi. Bir görüntü sisteminin uzamsal çözünürlüğü, sistem hassasiyeti ve her birinin tasarım ve etkilenme sürecinde optimize edilmiş kendi faktörlerine bağlı olduğu görüntü kalitesi ile tanımlanan bir PET sisteminin performansı. Bu araştırmanın amacı, alanda isteğe bağlı dedektör sınıfı olarak tanıtılan seryum katkılı alkali toprak parıldayan kristalleri kullanan yüksek performanslı beyin PET tarayıcısını tasarlamak ve simüle etmektir. Sistem GATE kullanılarak tasarlanmış ve uygulanmıştır ve performans NEMA NU4-2008 standardına uygun olarak değerlendirilmektedir. Simüle edilmiş tarayıcı sistemi, sırasıyla 320 mm ve 280 mm maksimum ve minimum iç yarıçapına sahip silindirik bir geometriye sahiptir. Silindir 58 başlığa ve 1 x 1 x 10 mm3 voksele ayrılmıştır, tarayıcıda toplam 435.000 voksel varken, stronsiyum hafinat (SHO), lutetium hafnat (LHO) ve baryum hafinat (BHO) olmak üzere üç yeni malzeme ile simüle edilmiştir. ve karşılaştırma için lutetium Oxyorthosilicate (LSO) ile. SHO, LHO, BHO, LSO sistem performansı, mm cinsinden ilgili sintilatörler için eksenel olarak FWHM 1.13 mm ve 1.18, 1.10, 1.11, 1.12'de ölçülen ortalama bir uzamsal çözünürlüğe,% 5.13,% 8.34, 6.51 mutlak hassasiyete sahiptir Sırasıyla% 5.83 ve sistem SHO, LHO, BHO, LSO için sırasıyla%13.2, 13.19% 13.19,% 6.63 ve% 13.27 dağılım oranına ve% 13.2 ortalama dağılım dağılımına sahiptir. Sonuçlar, önerilen sintilatörlerin yüksek performanslı beyin PET görüntüleme ve diğer radyasyon saptama uygulamaları için ümit verici dedektör sınıfları olarak değerlendirilebileceğini göstermektedir.

Anahtar Kelimeler: PET; beyin kanseri; scintillator; KAPI

TABLE OF CONTENTS

LIST OF TABLES

LIST OF FIGURES

LIST OF ABBREVIATIONS

1D:	One Dimensional
2D:	Two Dimensional
3D:	Three Dimensional
APD:	Avalanche Photo Diodes
ATP:	Adenosine triphosphate
BGO:	Bismuth Germanate
Br:	Bromine
C:	Carbon
CdTe:	Cadmium Telluride
CFOV:	Centre Field of View
CST:	Central Slice Theorem
CT:	Computed Tomography
CZT:	Cadmium Zinc Telluride
DC:	Direct Current
DOI:	Depth of Interaction
F:	Fluorine
FBP:	Filtered Back Projection
FDG:	Fluoro Deoxy Glucose
FOV:	Field of View
FT:	Fourier Transform
FWHM:	Full Width at Half Maximum
FWTM:	Full Width Tenth Maximum
GATE:	Geant4 Application for Emission Tomography
Ge:	Germanium
GSO:	Gadolinium Oxy-Silicate
I:	Iodine
IIR:	Iterative Image Reconstruction
KeV:	Kilo electron Volt
LM-OSEM:	List Mode-Ordered Subset Expectation Maximization
LOR:	Line of Response

LSO: Lutetium Oxyorthosilicate
LuAP: Lutetium Aluminum Perovskite
LYSO: Lutetium Yttrium Oxyorthosilicate
MC-PMT: Multi-Channel-Photo Multiplier Tube
MLEM: Maximum Likelihood Expectation Maximization
MRI: Magnetic Resonance Imaging
N: Nitrogen
NaI: Sodium Iodide
NEMA: National Electrical Manufacturers Association
O: Oxygen
OE: Origin Ensemble
OSEM: Ordered Subset Expectation Maximization
PET: Positron Emission Tomography
PMT: Photo Multiplier Tube
PSF: Point Spread Function
PS-PMT: Position Sensitive-Photo Multiplier Tube
RAMLA: Raw Action Maximum Likelihood Algorithm
RC: Recovery Co-efficient
SF: Scatter Fraction
Si: Silicon
SiPMs: Silicon Photo Multipliers
SNR: Signal-Noise- Ratio
SPECT: Single Photon Emission Computed Tomography
SR: Spatial Resolution
TOC: Transparent Optical Ceramic
TOF: Time of Flight
USPAP: United State Patent Application Publication
UV: Ultraviolet Visible
WB: Whole Body

CHAPTER 1
INTRODUCTION

Demands for high-performance diagnostic systems and techniques have increased in brain cancer and other mental diseases pattern studies. This happens due to growth in complications and consequences encountered from cancer and mental disorder severity. Among the most important medical imaging modalities required for functioning in clinical researches, positron emission tomography (PET) is at the top of the list (Vanquero and Kinahan, 2015). The operating principle based on the annihilation of positrons pair detected by a special detector to localize the dispersion of the radionuclide activity emitted from the patient (Sweet, 1951). During the last decennia, PET has become highly utilized in the medical field due to its ability to trace molecular activity and reveal the metabolic process of tissues.

Various research works aimed at developing a better performing brain PET scanners are on-going and these researches are being motivated by an increasing interest in functional images to aid early detection of brain tumors and other diseases (Vandenberghe et al., 2016). Among the deciding factors for PET performance is the detector element implemented which is characterized by quantum efficiency, stopping power, energy resolution, cost, timing resolution, and light yield (Venkataramani et al., 2003).

The most frequently employed detector elements used in the PET system are scintillating materials which have the property of emitting light when exposed to radiation in a process taking nanoseconds. The produced light wavelength ranges from visible light to UV spectrum suitable for processing the data in the photodetectors converting to an electrical signal (Melcher, 2000). The older scintillator is sodium iodide with thallium dopant (NaI (Tl)), disclosed to the world by Hofstadter in 1948 (Hofstadter, 1948). Due to its good light yield, it becomes known scintillator in the field of radiation, even if it has some pitfalls like poor detection for energy above 200Kev (Melcher, 2000).

The low detection efficiency at the expressed energy is mainly due to NaI (Tl) has low density. Among the scintillation materials currently in the field, Lutetium Oxyorthosilicate (LSO) is the well realized and mostly selected material for PET along with the Lutetium yttrium Oxyorthosilicate (LYSO) as the frequently implemented scintillation material (Nassalski et al., 2007). Radiation monitoring device incorporated in 2005 and United States Patent Application Publication (USPAP) in 2003 presented a report on class of Optical transparent Ceramic (TOC's) scintillators including cerium doped alkaline earth hafnates, which characterize them as better scintillation property and performance in light yield, stopping power, and quantum efficiency (Venkataramani et al., 2003). For this study, we hypothesize the above scintillators perform better than conventional crystals in our proposed brain PET scanner. It is also reported that these materials have the required physical properties that make them fit and to be considered as good scintillating crystals (Van Loef et al., 2007).

Currently, Silicon photomultipliers (SiPMT's) are emerging as the new classes of photodetectors with great potential for implementation in PET design, for their high gain, working at small bias voltage, better quantum yield, comparatively reduced cost, and noninterference to a magnetic field (Herbert et al., 2007). Due to their performance, SiPMT's photodetectors with quadrant readout techniques are selected for this particular study. Body organ-specific PET designs appreciated in providing better quality image required for the clinical and research area mainly due to their small field view. Unfortunately, most of the PET available commercially are whole-body scanners and only some of them produced to address specific body parts (Watanabe et al, 2002).

This research presents a high-performance brain PET scanner implementing pixelated cerium doped alkaline earth hafnates scintillators. The brain PET scanner design and simulation are accomplished via Geant4 Application for Tomographic Emission (GATE) software. The national electrical manufacturing association (NEMA) provides different guidelines for testing and evaluating the performance of PET designs in terms of their sensitivity, image spatial resolution, system scatter fraction and other parameters. In this study NEMA 2008 standards performance evaluation for small animal PET is employed to examine its performance.

1.1 Problem Statements

- According to US cancer society report on brain tumors, mental disorders and related complications shows the severity level for the area has reached as the 10th leading contributor of death requiring focus by researchers and scholar to conduct an extended study in early detection and management (Brain Tumor, 2019).

- Human brain study needs a brain imaging system capable of providing superior performance which is not addressed by whole-body PET's.
- The demand for a scintillator having inclusive property showing high efficiency, good stopping power, high light output and short response time has been a problem for implementing a super performance brain PET imaging.

1.2 Goal and Objectives

1.2.1 General objective

- To implement high performance brain PET scanners employing highly pixelated scintillators made of TOC's scintillator using GATE software and evaluate the system performance following NEMA 2008 testing criterion.

1.2.2 Specific objectives

The specific objectives of this particular study are to:

- Design and simulate a high-performance TOC's scintillators based brain PET.
- Simulate a superior-sensitive brain PET and show the contribution it can make for the clinical and basic researches in the field.
- Evaluate the system performance using GATE simulation following NEMA NU4-2008 PET performance testing guideline.

1.3 Significance of the Study

- The implemented high-performance brain PET scanners play a major role for early detection and better prognosis of brain-related disorders and tumors.
- Open TOC's scintillators as a new category of PET scanner photon detectors and can be implemented for high-performance PET imaging systems.
- Shows Cerium doped alkaline earth hafnates scintillators as a potential and promising detector material for application in nuclear medicine and related studies involving the requirement of PET technology.
- The results obtained from this study can be a contributor to brain imaging research and used as a baseline for future researches and studies.

1.4 Scope and Limitation of the Study

- The test performed following the NEMA 2008 standard to show the applicability of the new class of scintillation material to design better performance brain PET scanner system. However, the research did not cover all the parameters listed in the guideline but approximated.
- The specification and design implemented are limited to computer simulation. Consequently, extended evaluations for practical implementation are needed.

1.5 Outline of the Thesis Work

The thesis work starts with chapter one by introducing the basics of PET imaging and required instrumentation component selected as part of the design. The chapter also incorporates problems motivated the researcher to conduct the study, objectives to be achieved, the significance of the study, scopes, and limitations. Whereas chapter two delivers a literature review and PET imaging principle extended to the state of the art. The succeeding chapter three explains about cerium doped alkaline earth hafnium oxide scintillators. In chapter four, system design, specification and simulation were discussed. Chapter five focused on results and discussion. Finally, the conclusion and recommendations of the research are presented in the last chapter.

CHAPTER 2
LITERATURE REVIEW

2.1 Principles of PET Imaging in Nuclear Medicine

PET imaging technique involves precise detection and localization of annihilation events occurring post beta plus decay from radionuclide labeled radio-pharmaceutics Figure 2.1. It applies necessary electronic signal and image-processing methods after the annihilation output gamma ray detected by a photodetector and converted into a suitable electrical signal via an appropriate device. The coincidences are sorted into a sinogram or projection data, which holds information about the annihilation event. These data's are further processed by image reconstruction algorithms to reconstruct the image in a tomographic manner (Mikhaylova, 2014). Radionuclide-labeled biochemical known as radiotracers because they trace the location where there are higher rates of absorption and consumption of the compound labeled with radionuclide source.

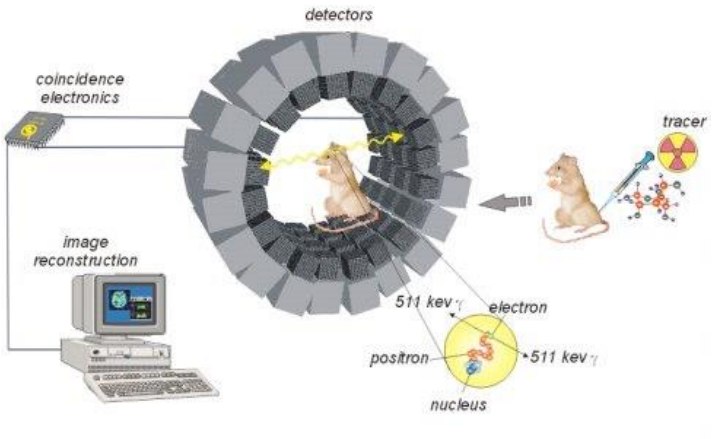

Figure 2.1: PET imaging process schematic representation (Bioimaging, 2014)

Most of the time in PET imaging ^{15}O, ^{11}C, ^{22}Na and ^{18}F labeled glucose radiotracers are applied for an imaging application. This is due to cancer cells utilize more glucose than the normal tissue cells (Jie Zheng, 2012). By injecting radionuclide labeled glucose, we can trace the distribution of glucose metabolism in the area through measuring the annihilation output gamma rays along with their geometrical relation. According to the pair production radiation tissue interaction process the annihilation of a positron from beta plus decay result into two photons along a 180-degree path back to back to each other Figure 2.2, this contributes for localization of the annihilation event and utilized in PET imaging.

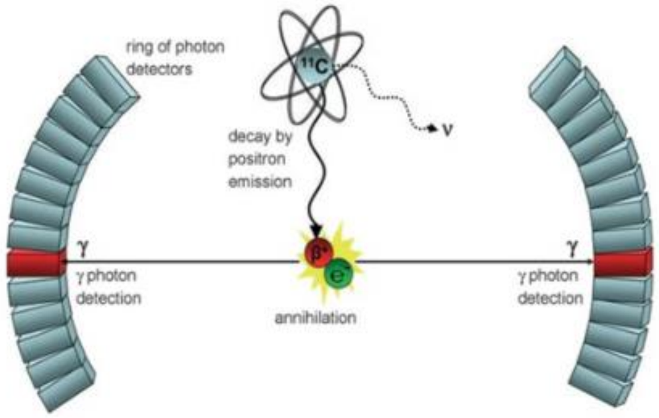

Figure 2.2: Schematic representation of the principle behind PET showing the positron decay and annihilation which produces two 511 Kev gammas (Miller et. al., 2008)

These photons are emitted at 511Kev of energy and categorical falls in the gamma-ray range of the electromagnetic spectrum. Their high-energy spectrum made them detectable outside the body without being absorbed by body tissue. Particularly, the localization of positron annihilation point is achieved through detecting these photons simultaneously thru photodetectors placed facing each other (Cherry et al., 2012).

2.1.1 Radiopharmaceuticals labeled with positron emitters

Nuclear medicine applications are interested in positron emitting decay processes due to the directional relationship and single nucleus emitting pair of photons. Some of the radionuclide isotopes frequently used in nuclear medicine are presented in Table 2.1.

Table 2.1: Property of radionuclides commonly applied for nuclear medicine imaging application (Cherry and Dahlbom, 2004).

Radionuclide	E_{max} (Mev)	Half-life (min)	Mean positron range in water (mm)
^{13}N	1.20	32	1.4
^{11}C	0.961	5.33	1.1
^{18}F	0.63	0.663	1.0
^{15}O	1.73	0.1-0.3	1.5
^{68}Ga	1.89	3900	1.7
^{82}Rb	2.60,3.38	1900	1.7

The above-mentioned radionuclides positron emitters can be labeled with atoms using the same elements containing compounds found at ground state which has biological importance. The result is radiolabeled biochemical compounds with the same property as the unlabeled one. Through the above-mentioned technique, several numbers of radionuclide labeled compound have been prepared for medical application (Cherry et al., 2012). Radionuclides applied in imaging application with a short half-life are produced via in house cyclotrons, unlike 18F having extended half-life compared with the above presented it can be used a few miles away from the production site.

The above-mentioned premises leads to a conclusion to have a cyclotron facility near the medical site. Most frequently applied radio pharmaceutics is glucose, FluoroDeoxyGlucose (FDG). Since glucose is a biochemical consumable by cells used as currency to prepare Adenosine triphosphate, (ATP) and distribution show the metabolic activity of the tissue. This gives good opportunity to detect diseases changing the normal energy consumption rate of the cell. Some of the diseases are epilepsy, neurodegenerative diseases, coronary artery, and cancer cell metastases.

Several radiopharmaceuticals exist with approval for medical and related study applications. Every radio-pharmaceutics has a specific aim in measuring its target process and the relation between the measured value and the applied radio-pharmaceutics is clear. A medical imaging system is implemented with the administered radio-pharmaceutics to localize their distribution in the body. The imaging system depicts the rate of consumption of the tissue, which gives very important information in characterizing the tissue. This achieved by taking several images in time function (Cherry et al., 2012).

2.1.2 Photon simultaneous detection

Simultaneous detection of photon produced as a product of annihilation from Positronium (positron-electron pair) is the underlying process of PET imaging. The resting mass of the positron and electron pair undergoes annihilation in producing a pair of photon aligned back-to-back 180 degrees. The emitted photon comprises equal energy of 511Kev. The photons displace few mm from the point of annihilation based on the energy and range of positron (Cherry et al, 2012). Through a technique of simultaneous recording the annihilated photons, PET is capable of locating the place where the process has occurred along the line of faced pair of detectors. In the process, there is no need for collimation.

The above process is known as coincidence detection. The ability of PET to localize the annihilation point could not be achieved without photons having enough energy to escape from the body and having a geometrical line of annihilation. Technically, the approach implemented in locating the annihilation point through the line joining detectors geometry is called electronic collimation (Cherry and Dahlbom, 2004). The recorded coincidences shown at Figure 2.3 are processed via coincidence logic. In PET imaging the logic for coincidence is implemented with electronics scheme of “time-stamp” for each event recorded.

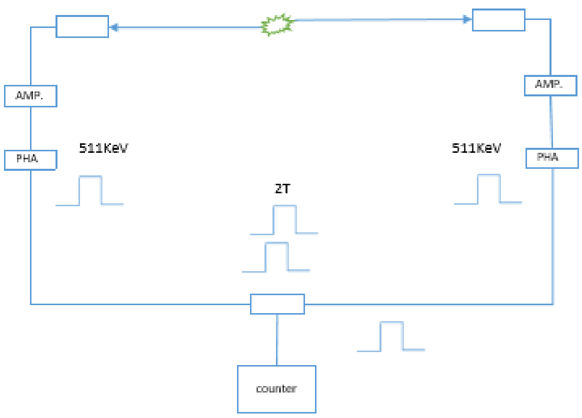

Figure 2.3: Coincidence logic circuit

The time-stamp concept is achieved in one or two nanoseconds (ns). The coincidence analyzer compares the time stamp of every event synchronically with the opposite side detector. To regard detected event as coincidence, it should be within the specified timing windows usually between 6 to 12 ns (Cherry et al., 2012). In relation to annihilation process, the obtained image can gate blurred due to non-collinearity defined priory as a slight deviation of photon path from 180 degree and displacement traversed by positron to find electron and annihilated to pair of photons (Cherry and Dahlbom, 2004). Positron range is the displacement from point of emission to annihilation point Figure 2.4. Even if it is not practical scholars suggest magnetic field can reduce positron range and enhance image resolution, the impracticality a rise from PET system sophistication.

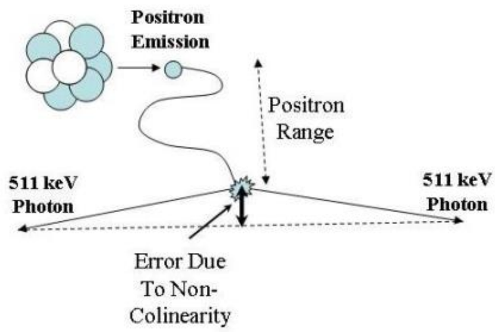

Figure 2. 4: Schematics of positron range and non-collinearity (Rahmim, 2006)

2.1.3 Time of flight

To locate the point of annihilation with a known amount of uncertainty some PET scholar suggested a technique called time of flight. It applies the time difference between coincidences recorded. This method assists image reconstruction without the computational algorithm. Time of flight Figure 2.5 assume given that time of arrival Δt, it is possible to find the annihilation point Δd with respective to detectors mid-point given by:

$$\Delta d = \frac{\Delta t x c}{2}$$

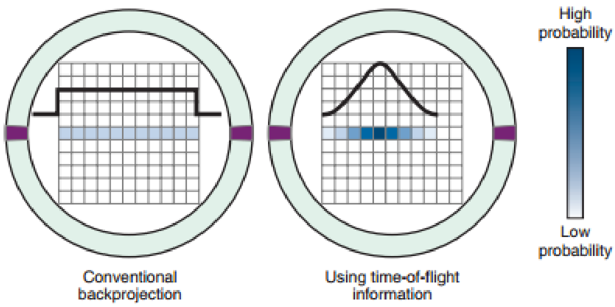

Figure 2. 5: Time flight versus conventional projection (cherry et al., 2012)

Where C is the speed of light in vacuum 3x108 m/s. With the current PET imaging technology time of flight, the method remains theoretical. For example, to achieve 1-cm resolution, we need a detector with a time resolution of 66 picoseconds. As a matter of fact these days we do not have such scintillator suitable for the time of flight PET imaging consequently, it makes the technique impractical (Cherry et al., 2012).

2.1.4 Annihilation coincidence event types

The recorder logic for coincidence results in annihilation detection output whenever a pair of coincidence arrival within the specified timing window. The coincidence events detected by the logic can be categorized into three main groups Figure 2.6. A coincidence event is labeled as true if the promptly detected pair of photons are from the same annihilation point between the detectors. True coincidence measures the system sensitivity in PET imaging. The coincidence detected on two different detectors within the viable time window accidentally but, the photons detected are from unrelated annihilation point we call such situation random/accidental coincidence event. These coincidences contributing to lowering image resolution and measurement accuracy. In case one of the photons taking a path from the annihilation point may gate interaction with tissue and deviate from the theoretical 180-degree alignment recorded as scattered coincidence, given that the time windows is maintained.

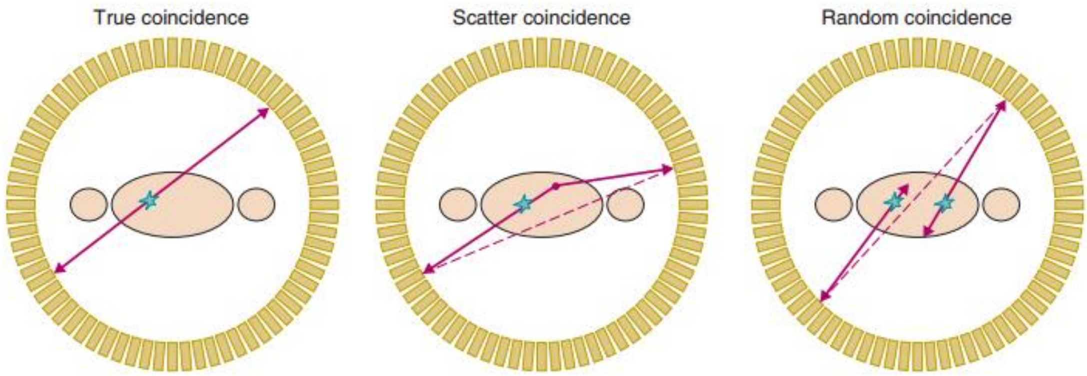

Figure 2.6: Schematics of coincidence event types (Cherry et al., 2012)

The scattering event can also arise from the interaction between the photon and scanner components outside the body (Cherry et al., 2012). The scatter coincidence represents the Compton scattering mode of photon particle interaction. It results in the scattered photon to lower in energy than the other traveling without interaction. Category of coincidence events also includes multiple or triple events. Triple coincidence arises during the detector records three events from two annihilation locations. For typical PET systems, the ratio of random to true coincidence event ranges from 0.1 to 0.2, scatter to a true event in brain imaging span from 0.2 to 0.5 and 0.4-2 for abdominal imaging (Cherry et al., 2012). Except for the true/ prompt coincidence the rest arise from scattering and unrelated annihilation process considered as a source of noise and image blurring (Bailey et al., 2005).

2.2 Data Acquisition in PET

2.2.1 Two and three dimensional data acquisition

In a PET imaging system, we may employ two modes of data acquisition methods (Cherry et al., 2012). Data can be acquired based on the implemented scanner and detector components, in two-dimension and three-dimensional setup. In two dimensional mode, the detectors are collimated axially or septa will be introduced between the detecting elements of a system component Figure 2.7. The septa efficiently intercept annihilation photons from scattered photons not to reach the detector surface. Not only contribute through the rejection of scattered photons but also random event by lowering the single—channeling recording amount. Which contribute to minimizing the dead time of the detector component and good signal to noise ratio (SNR).

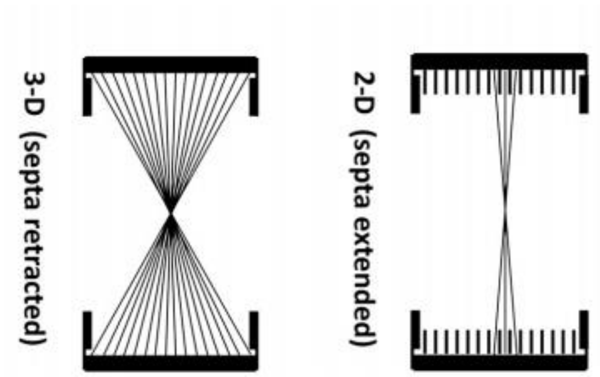

Figure 2.7: Schematics of 2D and 3D data acquisition (Terry and David, 2017)

To obtain photons from all possible line of response in a 3D mode of acquisition the septa placed within the detector ring are retracted. Such mode significantly improve the system sensitivity at the same time lead to elevated scattered and single-counting amount.

2.2.2 Coincidence data content

PET system can implement three forms of data organizing from the coincidence event detected by the system. List mode, frame and gate mode data sorting from the coincidence can be used. Starting from the later one, in gate method data collected synchronically with pulse or respiratory cycle. During the frame approach, it digitizes the position signal and moves in mapping the x-y points to image matrix. Acquiring image data will be altered followed by pixel value storage on a computer after a pre-allocated time elapse optionally after pre-settled counts. The naming frame implies to the single image data is acquired in frame series. It is important to allocate the size of the image matrix before beginning the acquisition. In list mode technique, which involves discretization and digitization of information regarding the coincidence event energy, time and location information. According to the designer choice, more information can be included in the list mode format. Comparatively this technique allows ease of acquisition at the same time it is not efficient in memory management for a typical PET system.

2.3 Photo Multiplier Tubes (PMTs)

Most of the PET available in the market utilize PMTs as a device to amplify the photons and produce an electrical current in relation to the amount of detected coincidence event (Cherry and Dahlbom, 2004). Figure 2.8 shows the schematics representation of the PMTs principle.

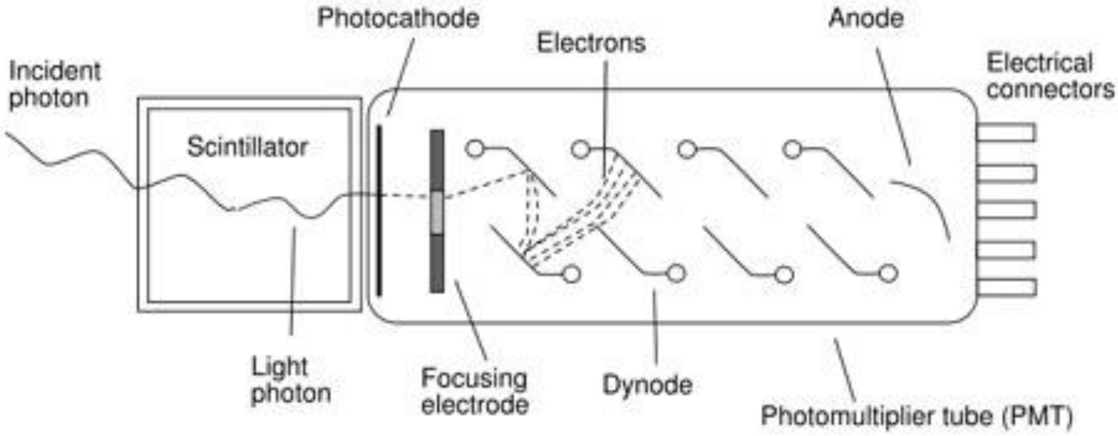

Figure 2 8: Schematics of PMT principle with scintillator coupling (Stanford, 2018)

Scintillator emits light and is directed to the PMT across a glass window which intended to excite the photocathode in turn. Energy deposition allows ease electron ejection as the cathode is thinly layered tailored for this task. The probability of ejecting an electron from the cathode material surface is known as quantum efficiency is in the range of 15% to 25% for scintillators (Knoll, 1999). The liberated electron accelerates toward the electrode by applying high voltage. The dynode or electrode is covered by suitable material ready for emitting electrons.

For single electron, 3 to 4 more electrons will be emitted from the surface of dynode. The process repeats throughout the PMT and ends up in nanoseconds with at least 106 of electron for a single one. Passing the amplification course the system has an adequate amount of electron to be processed. These devices exist in bulk with different size and shape. Most of them are characterized by limited quantum efficiencies and relatively higher cost.

2.4 Silicon Photo Multipliers (SiPM's)

SiPMs are promising photodetectors coupled with scintillators possibly in PET imaging (Herberta et al., 2007). It is known from their property semiconductors electrical property can be modified through doping external impurity. This possibility contributes to the process of photo detection and application in PET imaging. The process Figure 2.9 of detection and amplification of detected photon relies on the liberation of an electron as the silicon lattice encounter electron collision with sufficient energy.

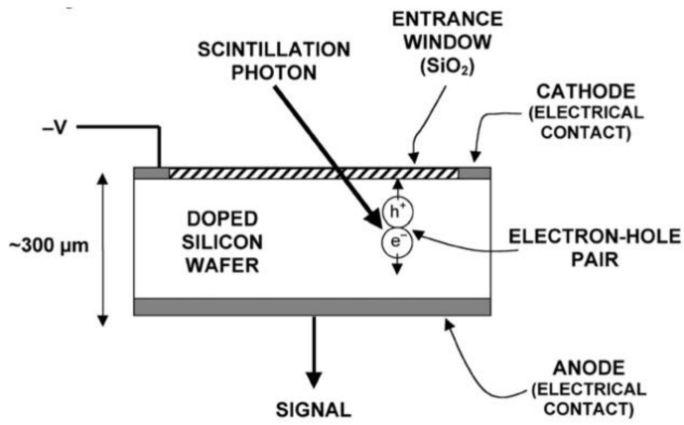

Figure 2.9: Photodiode process represented in schematics (Cherry and Dahlbom, 2004)

The potential difference applied externally allow drifting of an electron to the anode side while a hole the vacant move to the negative end of the cathode side. In the process, it creates a measurable amount of electrical current. SiPM's are characterized by a higher probability of electron liberation up to 60% to 80% (Herberta et al., 2007). On the other hand, they are criticized with their reduced internal gain. It produces only a single electron-hole pair per photon detected from the scintillator. Due to their poor internal gain, the produced signal has a lower strength than the counter PMTs. Even though they have weak signal they pose quick rise time, elevated gain in the range of 105 to 107 depending on the biased voltage, reduced noise, excellent energy resolution and immunity for magnetic field allowing hybrid imaging system implementation.

2.5 Avalanche Photodiode (APD)

There are an additional class of photodiodes with slight manipulation over their operation. They are operated at a higher voltage and through carefully selected operating temperature. These photodiodes are known for avalanche effect occurring due to the high operating voltage taking their character named as Avalanche photodiode. The voltage applied is intended for providing electrons with sufficient energy to liberate more electrons. In this class of photodiodes the gain depends on the potential difference and administered temperature. They are characterized by their enhanced SNR relative to solid state ones. APD's have gain ranging 102 to 103 and quantum efficiency in the same range as SiPMs. They are criticized for careful operation procedure requirement and bias voltage administration.

2.6 Image Reconstruction in PET

Point of annihilation is defined by drawing a line connecting the two detector elements. The line is known as Line of Response (LOR). The annihilation point is along the LOR. The other important term is projection, which is the accumulation of LOR recorded by the detector element with specific orientation angle. The two-dimensional sets of projection give sinogram Figure 2.10 of the image to be reconstructed.

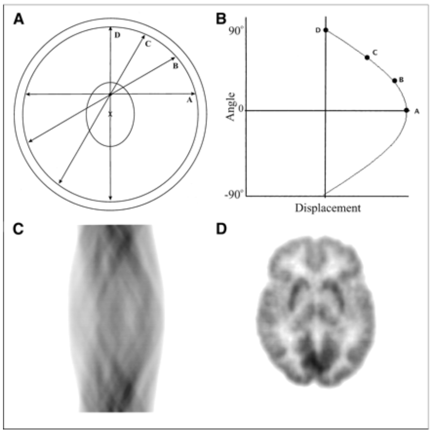

Figure 2.10: Schematics representing sinogram formation. (A) line of responses (B) projections (C) formed sinogram (D) reconstructed image (Frederic et al., 2002)

The recorded coincidence are accumulated as sinogram before the image is reconstructed by the appropriate image reconstruction. Practically, it feasible to develop 3D radionuclide activity distribution by cascading the 2D developed slices of tomographic images. In the next section of this discussion, we will see image reconstructions algorithms. They are classified as the analytical and iterative method.

2.6.1 Analytical methods

2.6.1.1 Filtered back projections

In 1967 Riddle and Bracewell presented image reconstruction approach known as filtered back-projection (FBP) analytical in nature involving filtering in the frequency domain. The FBP is widely used due to low processing time and fast reconstruction because it does not require iteration to be performed.

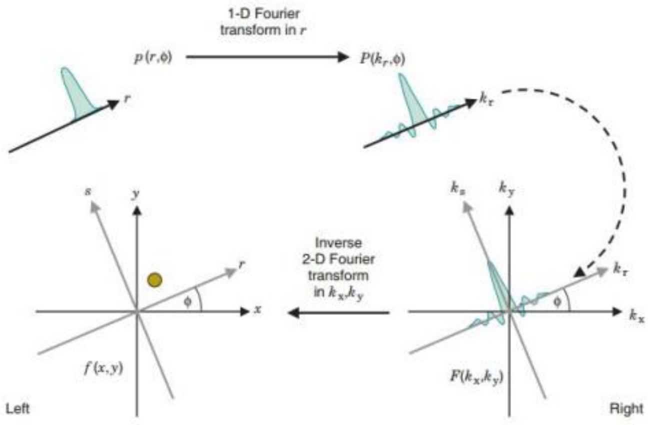

Figure 2.11: Basics of filtered back projection Fourier slice theorem. Fourier transform (left) and profile from 2D Fourier space (right) (Cherry et al., 2012).

The FBP is summarized as follows. Obtain projections in N different angles, compute 1D Fourier transform based on central slice theorem (CST) this provide us the 2D Fourier transform of the object in k-space. In the next step filter the projections in the k-space with a low pass filter (Shepp-Logan, Hann, Hamming, etc.). Compute inverse Fourier transform to have filtered projection profiles and finally, apply a conventional back projection Figure 2.12 to obtain the approximation of the radiopharmaceutical distribution in the body.

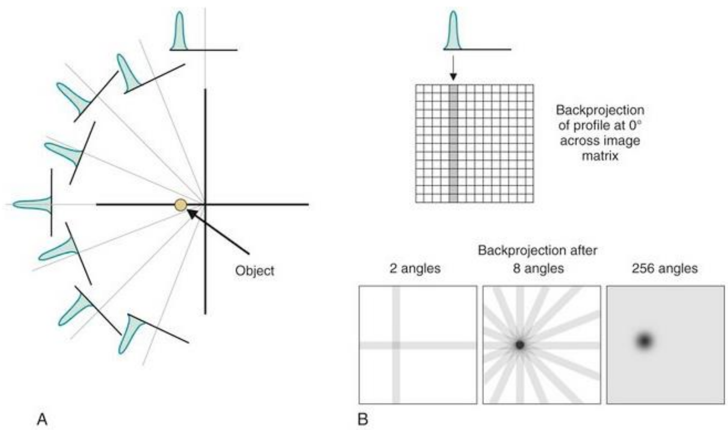

Figure 2.12: Illustration of simple back projection. (A) Projection profile at different angles, (B) simple back projection operation of intensity profiles. (Cherry, 2016).

NB: Many angles has to be included to have better approximation to point from different angle projection profiles.

2.6.1.2 Direct Fourier transform

The theorem of projections as shown on Figure 2.11, also called CST facilitates the process. Stated as, performing the Fourier transform on the projections of a 2D object along certain orientation, is the same as having the objects frequency value along with the origin in the same orientation. At the beginning calculate one-dimensional Fourier transform of the projections data. Keep the process by placing the filtered projections in a polar grid. Each projection in its corresponding angle. Then resample these in a Cartesian grid with interpolation (linear, nearest, splines, etc.). Finally, calculate the two-dimensional inverse Fourier transform, and obtain the reconstructed image.

2.6.2 Iterative image reconstruction

IIR approach achieved a high desire for image reconstruction because of their amenability, and realistic models of systems. They are able to show the appropriate mapping of sources to the recording eventually, contributing to creating high-quality images (Tohme and Qi, 2009). These methods are expensive in terms of computation cost, due to this it takes longer to be applied extensively in the tomographic reconstruction area until computation power of the computer has been improved through different performance-enhancing approaches. The basics behind IIR technique Figure 2.13 is the true measurement can be achieved through iterative approximations.

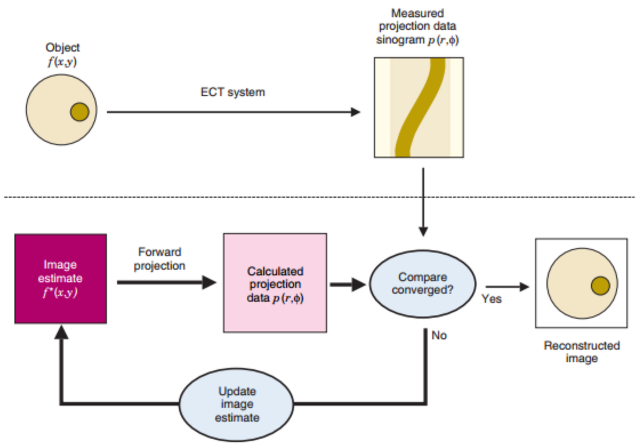

Figure 2.13: Schematic representation of iterative image reconstruction basics (Cherry, 2016)

Usual the initial approximation is taken to be a blank image. Then the recorded projections will be forward projected in a contrary to back projection task. The forward projection is accomplished by integrating the value across the projections. Then compare with the sinogram acquired during the imaging process. By setting a certain threshold deviation level keep comparing and updating till the error minimized to the pre-settled threshold value.

2.6.2.1 Maximum Likelihood Expectation maximization (MLEM)

These techniques follow the iterative approach to reconstruct the image from the recorded projection data. It implements a statistical approach to the approximate distribution of the source. The statistical estimation based on the maximum likelihood principle. In the process, it takes in to account the impact of counting stat. They are known for labeling a greater weight to high-count and reduced weight for low-count, the name was also given from this approach ML_EM. The reconstruction process is given by

$$I(w) = \sum_{u} N(\,u, w)\, P(w)$$

Where $I(w)$ is measured intensity in the w^{th} projection, $P(w)$ activity in the w^{th} pixel, $N\ (u, w)$ probability of activity emanated from u^{th} pixel will be detected in w^{th} projection. This approach is applied to find solution for inadequate information problems. Even if this technique has firm convergence and predictability it is criticized for noisy output and poor convergence rate. Once the matrix of $N_{u,w}$ determined the $(t+1)^{st}$ iteration of the EM can be given as:

$$P(t+1) = \frac{\mathrm{P}(t)}{\sum_{w} N\ (u, w)} x \sum_{w} N\, u, w\ \frac{\mathrm{P(w)}}{\sum_{l} N\ (l, w)\, \mathrm{P}(t, l)}$$

Where t is the iteration and $\sum_{l} N\ (l, w)\, \mathrm{P}(t, l)$ is the accumulation of image pixels computed before the process is implemented.

2.6.2.2 Ordered Subset Expectation Maximization (OSEM)

It is shown that ML_EM has expensive computing power (Tong et al., 2010). OSEM is suggested to solve this problem. It implements subsets for updating the image with a full set of information. This approach follows dividing projections with subsets classes of non-overlapping. From all of the classes of subsets, projections are integrated into the single subset by projecting back. In every sub-iteration update is applied to the image. There is another class of OSEM implementing list mode data format LM_OSEM. Literature suggest LM_OSEM as better than existing image reconstruction algorithm by applying fuzzy PROMETHEE (Ozsahin *et al*., 2018). It implements detected event instead of detector bins for recursive updating method. Because of the enormous amount of pixel found in the imaging system FOV which contributing to detected coincidence event the algorithm takes longer time to converge (Kolstein et al., 2013; Uzun et al., 2014).

2.7 Related Works

In this chapter, we will try to review the works related to our topic. The inception of PET technology evolution dates backs to 60 years from now including radionuclide labeled biochemical preparation. The advancement leads to rising of innovative brain PET scanners. The following literature review presents articles in chronologically order from the older one to recent studies in the area. It has confirmed that researchers in the field had made progress in brain PET imaging by implementing different geometry and scintillating materials.

Freifelder et al., (1994) among famous researchers in brain PET imaging presented HEAD PENN-PET design. The team aimed at achieving super sensitive and high spatial resolution scanner for clinical and research applications in neurophysiology. The presented study implemented 3D imaging by utilizing a NaI (Tl) detector. The system has 25.6 cm field of view. The spatial resolution measured from ramp impulse response presented 3.7 mm full-width half maximum (FWHM) in the both transverse and axial direction. The evaluated sensitivity of the system is about 50 kcps/pCi/cc/axial-cm peak.

Watanabe et al., (2002) one of the researchers in the field presented a study performed to improve the resolution of brain PET. The system characterized by 8x4 mm array of bismuth germanate (BGO), 2.88x6.55x30mm3 detector element, and 330mmx160mm scanner field of view. The reported was performance 2.9mm spatial resolution in the transverse and axial direction and two-dimensional sensitivity measure of 6.4Kcps/KBq/ml. Watanabe tells us the system has been commissioned for clinical implementation after passing through pre-clinical trial.

Wienhard et al., (2002) studied brain PET through designing octagonal shaped eight panels arranged in 35cm inner diameter and 25.2 cm height cylinder. The detector element dimensioned to be 2.1 × 2.1 × 7.5 mm3 implemented via LSO scintillating crystals. The system characterized by 4.3% absolute sensitivity and less than 2.8 mm spatial resolution measured at FWHM for 10mm sliding from central FOV and 2.4 mm at the central field of view (CFOV).

S. Karp et al., (2003) has developed G-PET for brain imaging with the same scanner as HEAD Penn-PET with an improved bore size of 42 outer and 30.0 cm inner cylinder and height of 25.6 cm geometry. The presented study implemented GSO (gadolinium Oxyorthosilicate) as a detector. The selected block size is 4x4x10 mm3. Applying the NEMA testing standard the developed system achieved 4.0 and 5.0mm spatial resolution in the transverse and axial direction at FWHM respectively. Using their own source and phantom geometry the study finding depicts that absolute sensitivity is 4.79 cps/KBq at 39% of scatter fraction.

S´eguinota et al., (2004) from European nuclear research institute presented high-performance cerebral PET scanner with cylindrical geometry of inner diameter of 35 cm and an outer diameter of 38 cm implemented and tested for performance following appropriate guideline and procedures. S´eguinota selected LSO and LaBr3 as detector element and resulted in a spatial resolution measured at the CFOV of 1.85 mm and 1.59 mm in Transverse direction and 5.78 mm and 3.43 for LSO and LaBr3 in axial direction respectively. The performance test shows good performance and possible implementation for clinical trial and research projects.

Mikhaylova et al., (2014) studied seamless PET design based on voxelized design implementing CdTe semiconductor detecting element. The study aims to crack the PET shortcoming by employing a 1x1x2 mm3 detector size. The developed PET has a sensitivity of 21 cps/KBq at 0.73 and 14 cps/KBq at 3.95% scatter fraction based on the NEMA NU 2-2001 guideline. The team concluded that voxel-based design shows superior performance over the existing PET designs.

Gong et al., (2016) implemented a crystal size of 2.5 x 2.5 x 20 mm3; with an axial gap of 2.5mm and axial field of view 190 mm. The research team presented high sensitivity for full helmet design approximated to 4.2 fold from cylindrical PET. The scatter fraction comparison show helmet design 31.2% scatter fraction using GATE simulation software. The article claims the image resolution significant improvement due to elevated sensitivity by including the depth of interaction and time of flight approach to localize the point of annihilation.

So far we have surfed progress made by researchers in tackling the quest for high-performance brain PET scanner through different geometries and scintillators, they lack in solving the problem by producing high resolution and developing a super sensitive system through manipulating geometries and implementing high pixelated new detector elements.

2.8 State of the Art

Present day introduced brain PET scanners employ a cylindrical geometry and scintillation crystal for coincidence photon detection. Recently, Watanabe et al., 2017, reported a high-performance brain PET scanner employed using the cylindrical scanner of 330mm trans-axial FOV and 201.9mm axial FOV through a fine segmentation of detector elements down to 1.2mm and implemented using LYSO scintillator. The system has a total of 655 360 crystal elements, 168 rings of a detector having a 1.2mm pitch, and an 8x8 array of photon recorder. The performance reported depicts that the system has 1mm spatial resolution measured at FWHM transversally and sensitivity of 21.4 cps/kBq tested using 18F line source. The image was reconstructed via one of IIR approach, list-mode dynamic RAMLA (LM-DRAMA) algorithm. Scintillators based PET also has been employed for Breast specific imaging system with excellent performance (Musa, Ozsahin and Ozsahin, 2018).

Some research teams are trying to crack PET imaging performance by implementing semiconductor detectors. Among them, Morimoto et al., 2011, came up with PET implemented via CdTe semiconductor detector dedicated to brain and neck region imaging. They have presented the system to possess an energy resolution of 4.1% at FWHM and timing resolution of 6ns. The performance test follows NEMA 1994 and the team claim that they have achieved 2.3mm spatial resolution at FWHM and 25.9 cps/KBq system sensitivity. The implemented system has 39% scatter fraction at 350-540KeV and 23% at 450-540KeV energy window. Currently solid state detectors are not only employed in PET but also in small animal SPECT system. Solid state detector like CsI: TI and reporting encouraging results by literature (Uzun-Ozsahin *et al*., 2016; Ozsahin *et al*., 2017).

In spite of most current systems employ conventional coincidence localization approach there are researches ongoing to implement TOF technique. The current state of brain PET imaging technology not bound in improving PET only it aims in hybrid imaging to have a system of multimodal scanners like PET/MRI and PET/CT for better diagnosis and disease management.

Researchers has evaluated nuclear medicine devices in their respective performance parameters PET, SPECT and hybrid systems and found out to be operating quite well (Ozsahin *et al*., 2017).

2.9 Photodetectors

Materials with a sensitive property upon exposure to high energy radiation are used in the application for characterization and sensing in PET imaging. As the radiation is intercepted by the materials surface their special response is used in picking up radiations. The most common photodetectors used in medical and high-energy physics application are scintillators, semiconductors, and gas-filled detectors. The application spectrum range from photons position and time measurement to photons interaction count. Some of the photodetectors are discussed below.

2.9.1 Solid-state detectors

Field of medical imaging is progressing so far by introducing new techniques and classes of detectors. Solid-state detectors family introduced in medical imaging as an alternative to scintillators. They are characterized by their excellent energy resolution. Because of their natural energy resolution, they are hunted for industrial and medical imaging applications. Even though they have interesting energy, resolution for application in medical imaging their spatial resolution efficiency found to be at the same level as scintillators can achieve. This happens because resolution mainly relies on the physical geometry of the detector. The way they detect a photon is a result of ionizing radiation absorption and in turn, the absorbed energy creates electrons movement toward conduction band leaving electron-hole at the valance band. The amount of electron-hole pair gate bigger as energy absorption still exists. To preserve the charge and alter recombination it needs an application of electrical potential difference through electrodes (Knoll, 2010). Finally, an electric signal will be generated for processing by the interfaced electronics. According to literature cadmium telluride and thallium bromide are among the most suitable material for high sensitivity and pronounced spatial resolution implementation (Ozsahin *et al*., 2019). The most applicable solid-state detectors are presented below Table 2.2 with their property and comparison between the scintillator and solid-state detector. They are used in different nuclear medicine system design including Compton cameras and breast imaging PET systems providing excellent resolution and performance (Calderon *et al*., 2011; Ozsahin and Unlu, 2014).

Table 2.2: Common semiconductor detectors and respective property (Knoll, 2010)

Property	Si	Ge	CdTe	CZT
Atomics number	14	32	48/52	48/30/52
Density (g/cm^3)	2.33	5.33	5.85	5.81
Band Gap at 300 KeV	1.12	0.663	1.44	1.6
Energy Resolution at 511Kev	0.1-0.3	0.1-0.3	1	2-6
Electron mobility (cm^2/vs)	1400	3900	1100	1000
Hole mobility cm^2/vs	450	1900	100	50

In comparison with scintillators, they are good at energy resolution, while scintillators have bad energy resolution comparative to semiconductors. They have a low atomic number, characterized by low quantum efficiency and pronounced cost. Comparatively, scintillators are cheap, exhibits good quantum efficiency and superior stopping power, as a result, their larger atomic number and density.

2.9.2 Gas filled detectors

Gas-filled based detectors operate by the principle of ionizing the gas molecules and measuring the current flow. They are among the oldest detectors in nuclear medicine application. During the gas molecules exposed to ionizing radiation, it gate interacted with gas molecule ionizing them in the process. The produced electron-ion pair will be in thermal random motion. Figure 2.18 show the schematic representation of the ionization chamber.

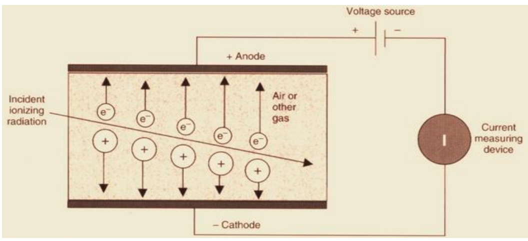

Figure 2.14: Schematic representation of ionization chamber (Radiologykey, 2016)

The randomly moving electron-ion pair may undergo charge transfer and recombination collision unless we apply the external electric field. Finally, the ionization current is measured to characterize the radiation. To alleviate possible chemical reaction non-reactive gases are selected. So far, we have discussed the ionization chamber. We have two more types of gas-filled type detectors. The proportional counter is among one of the gases filled mode detector, operating with the same principle as ionization chamber differing in the strength of electric field applied.

Proportional counters use principles of gas multiplication to provide sufficient voltage by folding the number of ions produced. The introduction of the stronger molecule leads to larger kinetic energy in turn ionizing the rest of ions. It creates low mobility to the other side of the ions. According to scholars, proportional counters are known for their low efficiency (Kamal, 2014). The rest of the gas-filled detector is a Geiger Muller detector which operates at the elevated electric field from proportional counters. Geiger Muller detector is characterized by easy operability and low-cost availability. They have longer dead time mentioned as a pitfall of these detectors.

2.9.3 Inorganic scintillators

The last half-century brings inorganic scintillators to nuclear physics studies and made a significant move in advancing their operation and application (Weber, 2002). Scintillators introduction to the nuclear physics research field realized as serendipity since then demand for scintillators has increased for the clinical and research applications (Lecoq, 2016). Mainly they are applied for the detection of ionizing radiations (Princeton, 1982). Scintillators can be organic or inorganic and available in liquid, gas, and solid state (Melcher, 2000). The main concern of this paper is inorganic scintillator specifically cerium doped alkaline earth hafnates. Scintillators emerged as important detector passing through a historical timeline which can be categorized into three phases (Weber, 2002). From the beginning of the discovery, CaWO4 implemented after the x-ray introduction to the world (Edison, 1896). Uranyl salt utilized by Becquerel during the radioactivity discovery, and Crookes used ZnS in counting and detection of radioactivity near the end of this phase Rutherford applied ZnS for alpha particles study and proved their encouraging nature for high energy physics research (Rutherford et al., 1930). Later through the discovery of PMT’s scientist show their feasibility in PET imaging (Weber, 2002). The timeline for scintillator material discoveries presented in Figure 2.19 below discovery beginning after the discovery of the x-ray by Roentgen.

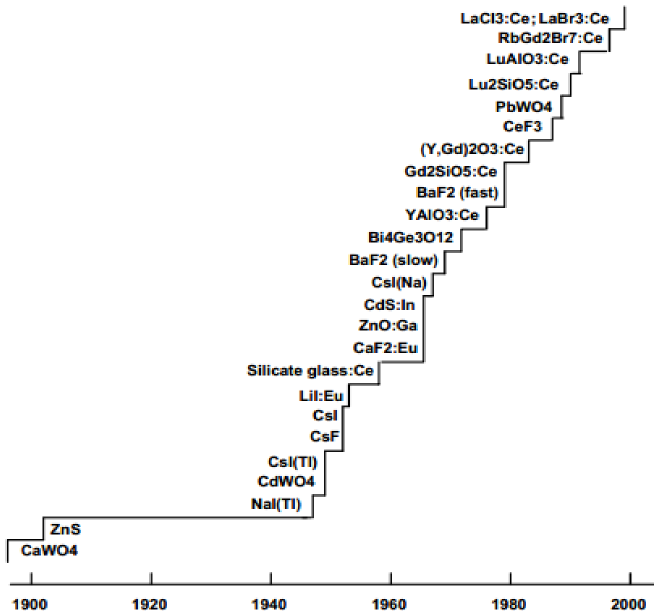

Figure 2.15: Inorganic scintillators discovery timeline (Weber, 2002)

In the second phase succeeding naphthalene discovery, Hofstadter has developed NaI (Tl) scintillator. The coming few years, alkali halide based scintillators studied and presented to the medical and research field. The third phase which is the last 20 years show us real growth and demand for research areas and industrial applications. Describing the chronological order of discoveries and studies, currently, we have an enormous amount of inorganic scintillators for different applications including ceramics, crystals, glasses, halides, and oxides (Knoll, 2000). Best scintillators are characterized by scintillation wavelength matching photoconductivity, adequate light yield, higher density giving better radiation stopping power, nice energy resolution contributing to a good resolution, shorter decay contributing for better time resolution and possible time of flight localization of activity, and availability of material and cost of implementation.

2.9.4 Operating principle of scintillation materials

A scintillator is a collective name given for materials giving off light in the range of visible light or UV spectrum following ionizing radiation exposure. Most of the scintillation materials implemented in medical imaging are inorganic ones.

The crystal lattice is the defining factor for a mode of scintillation, where specific energy band permitted to be occupied by electrons (Knoll, 1999). Electrons elevated to the conduction band leaving a gap at the valance band through the process electron returning back to the valence band result in photon release but not adequate. Width of the band gap contributes to the wavelength of the emanated photon to fall in the visible/UV spectrum (Knoll, 1999). Figure 2.20 shows the scintillation process for pure and activated scintillating materials, where impurity introduction to the crystal activates the crystal for better emission.

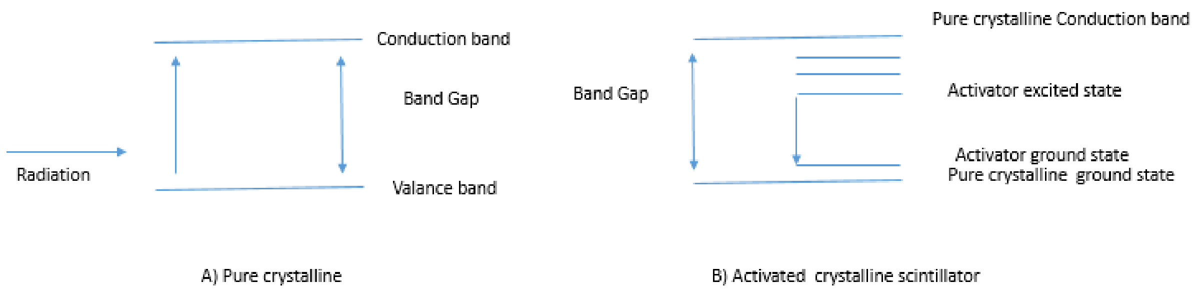

Figure 2.16: Energy band structure of an inorganic scintillator

To modify the band gap and energy structure in the scintillation crystals impurities are introduced. The overall process of scintillation categorized into three steps (Lempicki et al. 1993). At the beginning the incident radiation energy is absorbed and translated to thermally active electrons and holes, part of electrons and holes transferred to the center of luminescence and finally illuminate photon.

Ionizing radiation results in creating a charged particle to travel across the crystal material causing enormous electron holes. The activator site will be filled by drifting positive holes ionization. Due to this, electrons settled free to move across the material and keep doing this until they find an activation location that is ionized. The electrons jump to impurity location, forming impurity within the exciting status. With a possibility of an emitting photon the de-excitation, happen so quickly. Purpose of activating impurity is to shift the emitted photons in the visible light range. According to scholars half-life for typical activator ranges from 7-10s. Due to this duration of light output is decided by the half-life of the activator.

2.9.5 Scintillation efficiency

The scintillation efficiency is the ability of a scintillating material to convert the absorbed γ energy to photons. Table 2.3 presents ideal scintillators property.

Table 2.3: Ideal scintillator properties (Melcher, 2000)

Property	Description
High density	High stopping power
High light output	More crystals per photodetector
High atomic number	Higher rate of detection
Short decay time	Good coincidence timing
Good energy resolution	Clear identification of energy events
Emission wavelength in UV/Visible range	Match photomultiplier tube
Transparent emission wave length	Unimpeded light travel across the crystal
Index of refraction	Good light emission from crystal to photomultiplier
Radiation hard	Stable performance
Non-hygroscopic	Packaging simplification
Rugged	Smaller crystal fabrication
Economic growth process	Economic production good cost management

According to the table above several combinations of properties are required to be ideal scintillating material for high-energy physics studies and applications. Universally materials having a high atomic number and high density are demanding due to their pronounced stopping power and making the process to utilize lower amount scintillating material by volume (Weber, 2002). A scintillator needs to have a high atomic and higher mass to volume ratio to have better high-energy radiation detection. It is known that at the energy level of 511Kev the dominating interaction modes are Compton and photoelectric, requiring higher atomic number and good stopping power by the scintillating material. To have good timing of coincidences, which means having a brief photons pulse we need our scintillator to have shorter decay time. This improves our counting rate ability. The other quality we require is to have a high light output by the scintillating material. This makes arrangement of multi-crystal for a single photodetector lead to economical design and implementation. While selecting a detector for PET application having a narrow difference in energy detecting scintillator make us able to see all energy events in the process.

Since we are interfacing the scintillation output to photo-detectors, we require a material applied for scintillation to hold a refractive index around 1.5. For not impeding the light traveling process in the scintillator, we need the scintillator to have radiation hardness property. Some scintillators absorb water from the environment they reside, known as hygroscopic property (Melcher, 2000). For simplicity in packing, we need the material to be non-hygroscopic. The ruggedness of scintillators required in assisting to produce small-sized scintillators easily.

The scintillation efficiency is presented by a product of three entities. According to (Lempicki et al. 1993), the overall efficiency φ is given by:

$\varphi = \beta SQ$

Where:

β: $conversion\ efficiency, S$: $transfer\ efficiency\ the\ energy\ held\ by\ electrons$ and Q: $quantum\ efficiecny\ of\ the\ scintillator$

Scholar’s demonstrated β is achievable from physical properties of the scintillator (Robbins, 1980). Quantum efficiency is measured by direct excitation under UV. There is no established model to calculate the transfer efficiency S and this is the current challenge and researchers are working to develop a model. Efficiency of well know scintillating material at room temperature presented in Table 2.4

Table 2.4: Scintillating materials efficiency (Weber, 2002)

Property	Density (g/cm3)	Decay time (ns)	Photon/Mev	Wavelength (nm)	Efficiency (%)
CsI	4.51	980	2,000	315	0.8
NaI(Tl)	3.67	230	38,000	415	11.3
CsI (Tl)	4.51	980	65,000	540	13.7
LSO: Ce	7.4	40	25,000	420	7.4
CaF_2: Eu	3.18	950	24,000	435	6.8
$RbGd_2Br_7$: Ce	4.8	45	56,000	410	16.9
Gd_2O_2S: Tb	7.34	600	70,000	545	16.0
LaOBr: Tb	6.17	425	67,000	425	19.5
$CdWO_4$	7.9	480	15,000	480	3.6
$Bi_2Ge_3O_{12}$	7.13	300	8,200	480	2.1

From the table above activated materials depicts higher efficiency comparative to self-activated ones, this is due to Q goes low as a result of thermal quenching at 25oc room temperature (Weber, 2002). Cost of scintillating material per cubic meter is the decisive factor for affordable medical imaging modality design and implementation (Melcher, 2000). The cost includes the material cost in raw and the cost of production. As mentioned before inorganic detectors include ceramics and glass, known for their low-cost availability and mass production (Weber, 2002).

To this day in the progress of scintillator material development and advancement, no material found to be superior and fitting for every application in the research area (Derenzo et al., 1990). But, prevailing new scintillator and testing it is possible to simulate numerically and characterize them.

CHAPTER 3
CERIUM DOPED ALKALINE EARTH HAFNATE SCINTILLATORS

3.1 Cerium Doped Alkaline Earth Hafnium Oxide Scintillators

USPAP in 2003, presented cerium doped alkaline earth hafnate scintillators with potential for PET imaging and high energy physics applications. These new scintillators characterized by elevated stopping power, non-hygroscopic and relatively good light output (Venkataramani et al., 2003). Where these properties are desired for PET detector implementation. Not only this, they have fast decay time made them an area of interest for high-performance PET imaging system design (Edgar V.et al., 2007). Namely, they are cerium doped strontium hafnate (SrHfo3: Ce), cerium doped lutetium hafnate (Lu2Hf2O7: Ce), and cerium-doped barium hafnate (BaHfO3: Ce). They are also known as optical transparent ceramic scintillators (TOC's). The above-presented composition of materials contains cerium and hafnate with alkaline earth metals. They can be generalized with a formula AHfO: Ce, where the A denotes alkaline earth metal to be Sr, Ba, and Lu. The suggested atomic ratio A: Hf is 0.9:1 to 1.1:1. The dopant extent should be 0.005 in percent (Venkataramani et al., 2003).

3.2 Properties

Light emission wavelength range is among the important features of scintillators. This is required for interfacing their output to light amplifying devices, such as PMTs. The cerium doped alkaline earth based scintillators have emission range from 350 nm to 500 nm. Which comply with several PMT's operating wavelength range. To achieve this property we have to keep the composition ratio mentioned previously.

The light yield measured from BaHfO3:Ce is about 28,000 photons/MeV compared with BGO it 3 and half times better, where the light yield from SrHfO3: Ce recorded to be 45,000 photons/MeV which 5 folds from BGO, Lu2Hf2O7 yields the same grade as BGO during the test under x-ray (Michael, 2009). The decay time found to be 10-20ns (Michael, 2009). Figure 3.1.show the wavelength versus intensity of the light output plot to demonstrate scintillators property along with their specific refractive index showing Lu2Hf2O7 with higher transparency but lowered light intensity output.

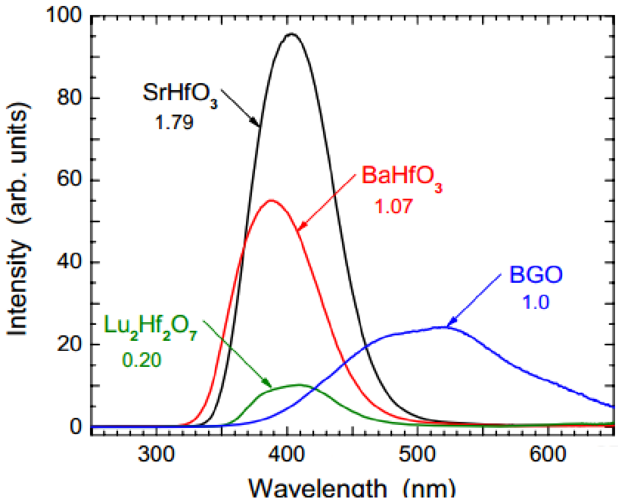

Figure 3.1: TOC's scintillators light output and emission wavelength range relative with BGO (Michael, 2009)

Their optical property is approximately isotropic lead us to have fully optical transparent ceramic (TOC's) scintillators, in turn, provides us a chance to create cheap and monocrystalline growth. From the above presented properties, we can take inference that these material are unique to demonstrate high density and relatively adequate light output, quick decay time and possibly taken us promising material for researches in nuclear physics and medical imaging application (Michael, 2009).

The research team who had claimed patent from USPAP described that the scintillation property of TOC's showed that they pose relatively high light output and shorter decay time. Additionally these materials because of their elevated density they demonstrated better-stopping power. Table 3.1.shows the relative property comparison between the existing scintillators and newly suggested TOC's scintillators.

Table 3.1: Cerium doped alkaline earth scintillators and exiting ones property (Venkataramani et al., 2003)

Property	**NaI(Tl)**	**BGO**	**Gd_2SiO_5: Ce^{3+}**	**Lu_2SiO_5: Ce^{3+}**	**TOC's**
Density(g/cm^3)	3.7	7.1	6.7	7.4	7.7-8.4
Attenuation coefficient at 511Kev (cm^{-1})	0.37	0.95	0.70	0.89	0.85-0.95
Relative light output (%)	100	7-12	30	30	20-30
Decay time (ns)	230	300	40	40	10-45

Michael J. Furey, 2009 from Brookhaven reported a study on TOC's focusing on SrHfO3: Ce morphology and optical properties. The study result shows it is possible to have transparent scintillator with a stoichiometric ratio of Sr: Hf ~1 and reasonably higher light output comparatively. Michael concluded that the possible implementation of these materials in PET imaging to be used as detectors. Van Loef *et al*., 2007, known for studying ceramic-based scintillators presented a paper on cerium doped strontium hafnates at the microstructure in transparency and radioluminescence.

Their findings show that the light output and physical properties are promising for medical imaging application and their scintillation properties are excellent comparatively to BGO. Beyond their scintillation property, the research team presented producing in huge quantity possible with a reduced cost they will be suitable to apply in nuclear medicine and considered an area of interest for PET and CT imaging. Van Loef and his research team at the same year reported that the scintillation property characterizing SrHfO3: Ce3+ and BaHfO3: Ce3+ scintillators emission wavelength comply with photodetectors without phase shifters application and inscribed in the study to be in the range from 410nm to 400nm. The decay time for the respective scintillators is reported to be 42ns and 25ns. The presented time resolution was 276ps measured at full width half maximum.

As we have discussed in the last chapter about the scintillators used in PET imaging are interested in the above-mentioned scintillators property and based on the literature review on TOC's scintillators, it is confirmed and we would like to propose these scintillators as promising detectors for application in medical imaging like PET and high energy physics.

3.3 TOC's Preparation

Production of the cerium doped alkaline earth hafnium oxide scintillators has three steps and extension for light transparency improvement. The first and the basic is preparing or affording the composition compounds. Then mixing with the appropriate ratio and firing under a certain temperature for a while. To achieve better light transparent scintillators extended powder pressing at elevated temperature is performed under isostatic condition. This helps in producing a polycrystalline with improved light transparency. The above-presented procedure makes us able to have cerium doped polycrystalline hafnates scintillating material. The alkaline earth metals are associated with oxygen instead of element-element relation. Where these materials are responsive to gamma-ray interaction result in improved light yield, fast decay time and appreciated stopping power (Venkataramani et al., 2003).

CHAPTER 4
SYSTEM DESIGN, SPECIFICATION AND SIMULATION

4.1 System Design and Specification

The brain PET designed and simulated in this thesis work mainly focus on implementing a novel class of scintillating material and show their applicability in high-performance brain PET imaging. In this study, the GATE simulation environment is used to appraise the performance of the specified brain PET scanner. The implemented TOC's scintillator has high stopping power and good conversion efficiency relative to existing inorganic scintillation crystals (Table 3.1). The system specified in this paper implement high pixelation in the crystals down to 1x1x10 mm3. The scanner also incorporates measurement in DOI due to crystals small voxel size. The system designed is flexible to be implemented for different scanner geometry for the whole body as well as to other organ-specific PET systems.

The simulated scanner system has a cylindrical PET with the geometry of a maximum radius of 320 mm and minimum inner radius of 280 mm. The cylinder is segmented into 58 heads of size 30 mm x 30 mm x 250 mm in x, y, z Cartesian coordinate respectively and within the head we have modules of size 10 mm x 30 mm x 250 mm in x, y, z respectively. Where the system has a total of 435,000 voxels dedicated to recording coincidences photon. System specification of the scanner is summarized in the form of a Table (Table 4.1) and schematically depicted in the figure below Fig 4.1.

Table 4.1: System geometry specification

System geometry	Specification
Crystal	LHO, BHO, SHO, LSO
Number of head	58
Module	1 cm x 3 cm x 25 cm
Voxel	10 mm x 1mm x 1 mm

NB: - LHO: cerium doped lutetium hafnate ($Lu_2Hf_2O_7$: Ce), BHO: cerium doped barium hafnate ($BaHfO_3$: Ce) SHO: cerium doped strontium hafnate ($SrHfO_3$: Ce).

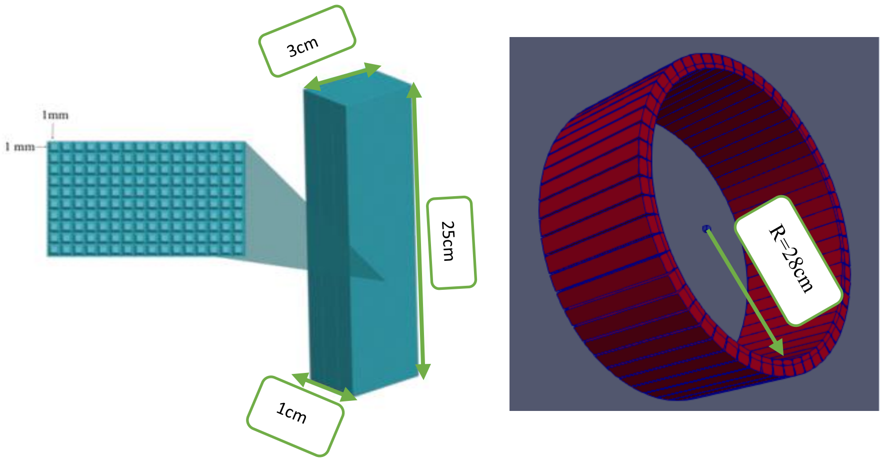

Figure 4.1: Schematics of the module (left) and cylindrical geometry of simulated scanner (right)

4.1.1 Monte Carlo simulation

Monte Carlo simulation involves enormous subsets of mathematical techniques implemented iteratively on random classes of samples. It mainly relies on the random way of problem-solving and allows testing of theoretical and practical systems. The simulation and analysis are accomplished by building a model and testing every possible scenario. Emission tomography uses the Monte Carlo simulation method in designing effective medical imaging systems, by applying reconstruction methods (şın *et al*., 2017), test scatters correction approaches and through enhancing scanning protocols. Even if Monte Carlo simulation applied in PET has slight pitfalls invalidation and accuracy, it appreciated for simplicity of implementation (GATE, 2016). Monte Carlo can be implemented in different programming tools including Microsoft Excel application, C, C++, Matlab, and other scripting languages. GATE is expatiated in the succeeding section where it is one of the C++ based Monte Carlo approach.

4.1.2 GATE

GATE is a validated simulation environment for nuclear medicine applications (Jan et al., 2004). The unique characteristics of GATE are its ability to manage phenomena's which are dependent on time (Staelens et al., 2003). GATE allows the ability to transform conceptual time-dependent activities into a model and simulate the phenomena, find out how entities interact and provide a realistic output. Accomplished through relating the source kinetics with the developed geometry of the system. The simulation environment is specifically tailored for nuclear medicine applications like human and small animal PET and SPECT systems.

The flexibility of the GATE allows the recursive implementation of GEANT4 libraries for a different scenario of simulation phenomena's in nuclear medicine. It allows different layers according to your level of knowledge. It extends from the application layer to a developer layer including a user layer being in the middle. The developer layer includes a core layer within it. The core layer of the GATE has different sub-layers incorporated along with it. Which allow from geometry development to physics entity interactions model definition and others. At the user level, the user is capable of running simulation with interactive scripts from constructing geometry to the end of running the full system model.

The designed system typically has a ring composed of modules constructed with blocks of segmented crystals. The scanner electronics component response is simulated in the "digitizer" of GATE element. To simplify the implementation of GATE to researcher and studies it incorporates benchmarks for simulation specific models and it includes examples of how to start with a simulation. The output information gathered from the GATE can also be compared with real data for validation purpose.

4.2 Performance Evaluation Parameters

Different standards for testing PET scanners system performance has been developed by NEMA. Which include the standard for WB PET and rat/mouse PET systems. To do the system performance evaluation, we have approximated the small animal PET system to apply in brain PET imaging system performance testing. In this particular research, in order to estimate the performance of the scanning systems, we followed the NEMA NU4-2008 standard procedure (NEMA, 2008). The data was collected following the standard and the image reconstructed via 3D direct Fourier method. During the entire procedure, the energy window was 350 – 650Kev, and a timing window of 10ns is set.

4.2.1 Sensitivity

The power of detecting coincidences in the FOV of the imaging system is described as the Sensitivity of the device under performance evaluation. The major contributors to the sensitivity of the system are the applied detecting element stopping power and the designed geometry of the imaging system. Sensitivity is reported as count per second per micro curie (cps/μci) or count per second per kilo Becquerel (cps/KBq). Equation (4.1) show relation among parameters of PET system design.

$$s = \frac{A.\varepsilon^2.\exp(-\mu t).3.7x10^\wedge4}{4\pi r^\wedge 2} \qquad \boxed{4.1}$$

Where A is the area observed by a point source, ε, detector element efficiency, μ, is the linear attenuation at 511Kev gamma photon of the detector material and t thickness of the detector finally, r is the ring radius. From equation (4.1) we can infer that system with a higher value of A which means having higher FOV in the axial direction and reduced radius of the ring can have greater power of detecting coincidence. According to NEMA testing standard the slice sensitivity if given by equation (4.2):

$$Si = \left(\frac{Ri - Rbi}{Acal}\right) \qquad \boxed{4.2}$$

Where R_i is the acquired count of the total at the specific and R_{bi} is the background counting and A_{cal} is the applied source activity for the testing procedure. S_i is the computed slice sensitivity. The sensitivity of the PET scanner is expected to be higher in the center of the FOV. Relative sensitivity of the system can be computed using equation (4.3).

$$S(A, i) = \left(\frac{Si}{0.9060}\right) x100 \qquad \boxed{4.3}$$

Where the number 0.9060 show the branching ratio of Na22. From now we can compute the total sensitivity by integrating the slice-based sensitivity of the system. The phantom and source applied in spatial resolution phantom are used in sensitivity test as shown in Figure 4.1. In the case of the simulation, the background count is taken to be none because we are running simulation in a computer program with no residual activity.

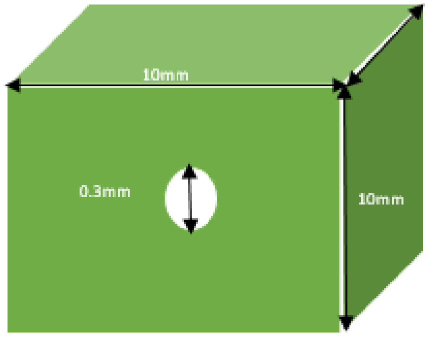

Figure 4.2: Sensitivity testing phantom acrylic cube

4.2.2 Spatial resolution

It is defined as the system's ability to differentiate points in the image. The evaluation for spatial resolution is computed from the reconstructed image of the point source. It shows the characteristics of images point spread function width measured at FWHM or full-width tenth maximum (FWTM). These measurements are performed in axial, radial, and transverse direction on a slice of the transversal plane. It is recommended to take a spatial resolution in the axial direction. The phantom applied for spatial resolution incorporate a point source of Na22 size not exceeding 0.3mm diameter to be measured at the CFOV with activity measured to be 24.5KBq imbedded in plexiglass acrylic cube of 10 x 10 x10mm3 size Figure 4.1. The minimum of amount prompt counts to be detected for spatial resolution is about 10^5 as recommended by NEMA NU4-2008 standard. To reconstruct the image we have implemented inherently 3D direct Fourier based algorithm with 0.5mm slice thickness.

4.2.3 Scatter fraction

Miss location of coincidence event can encounter as a result of scattering effect. The sensitivity toward scattered radiation depends on the implemented design of the scanner. SF fraction test is performed to identify the designed PET system sensitivity for scattered photon radiation. This characterization of the system is done at minimized counting rate aiming in reducing the effect of pileup, dead-time and random event. The mathematical computation is accomplished according to the equation given below.

$$SF = \frac{\sum_i \sum_{j'} C_{r+s,i,j'}}{\sum_i \sum_{j'} C_{TOT,i,j'}} \qquad (4.4)$$

Where Cr+s, i,j is the scatter counting, ith depicting the slice number and where j' show acquisition. Ctot is the total counting from the scattered and true counts. In this thesis work, we have applied the NEMA NU4-2008 scatter fraction test procedure. According to the guide, a cylindrical phantom of polyethylene Figure 4.3 with a dimension of 70 ±0.5mm in length and 25+/-0.5 mm in diameter is implemented. The testing document order a cylinder to have 3.2mm in diameter opening at a 10mm radial location and aligned in parallel to the d central axis. A 60 mm longer line source fitting the opening created previously is implemented.

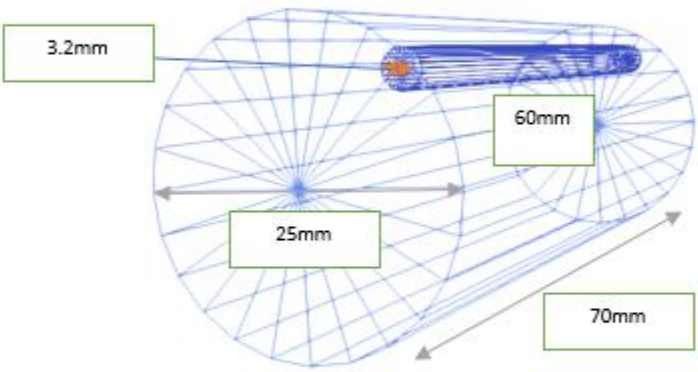

Figure 4.3: Phantom geometry for Scatter Fraction testing

The inserted line source is labeled with a certain amount of radioactivity fitted in the opening. As recommended by the testing document the selected activity has to be lowered to reduce the amount of random coincidence in limited record relative to the true coincidence. The testing phantom is located at the CFOV aligned in parallel to the z-axis. With the minimum recommended source activity we should have to record as much as 500,000 events. The implemented source type was to be ^{18}F.

4.2.4 Image quality

Image quality test is accomplished by implementing a phantom of poly-methyl-meth-acrylate having fillable five rods of size 1mm to 5mm. Rods and main body parts are filled using ^{18}F type radionuclide with 3.7MBq source activity. The phantom has a cold top section with a pair of chambers, where one with air and the other filled with water which able to create the cold section of the phantom Figure 4.4. Based on the implemented NEMA standard it requires about 10 million events to be recorded to reconstruct the image and evaluate image quality. Without any correction being implemented fully 3D direct Fourier reconstruction algorithm with 0.5mm slice thickness was implemented to recover the image.

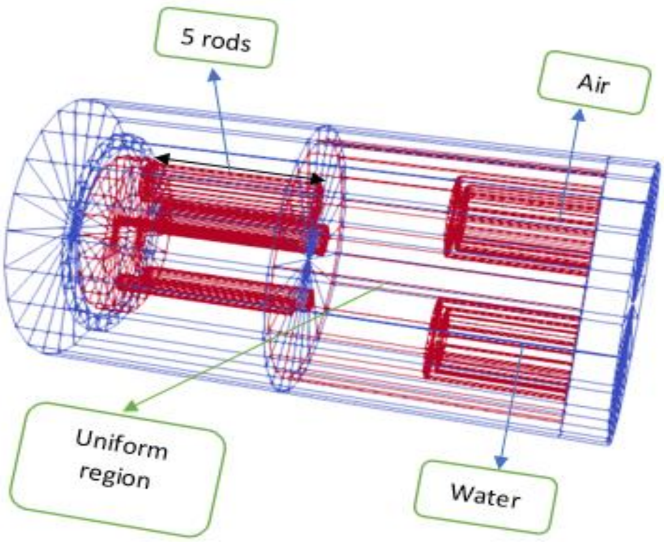

Figure 4.4: NEMA NU4-2008 Image quality phantom from Paraview

CHAPTER 5
RESULTS and DISCUSSION

5.1 Results

5.1.1 Sensitivity

The sensitivity test follow NEMA 2008 criterion and presents system ability to collect gamma ray at the selected energy window, specified source activity, and pre-settled timing window. Figure 5.1 presents sensitivity of the system for the suggested scintillating crystals, Figure 5.2 depicts sensitivity measured at CFOV presented in cps/KBq, and Figure 5.3 shows sensitivity profile across the axial FOV.

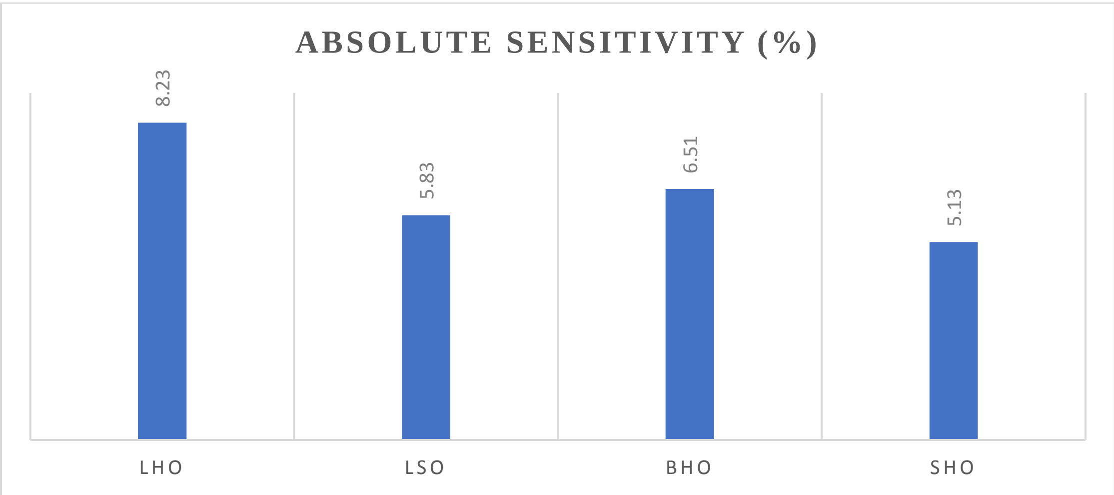

Figure 5.1: System absolute sensitivity for each implemented scintillating crystal

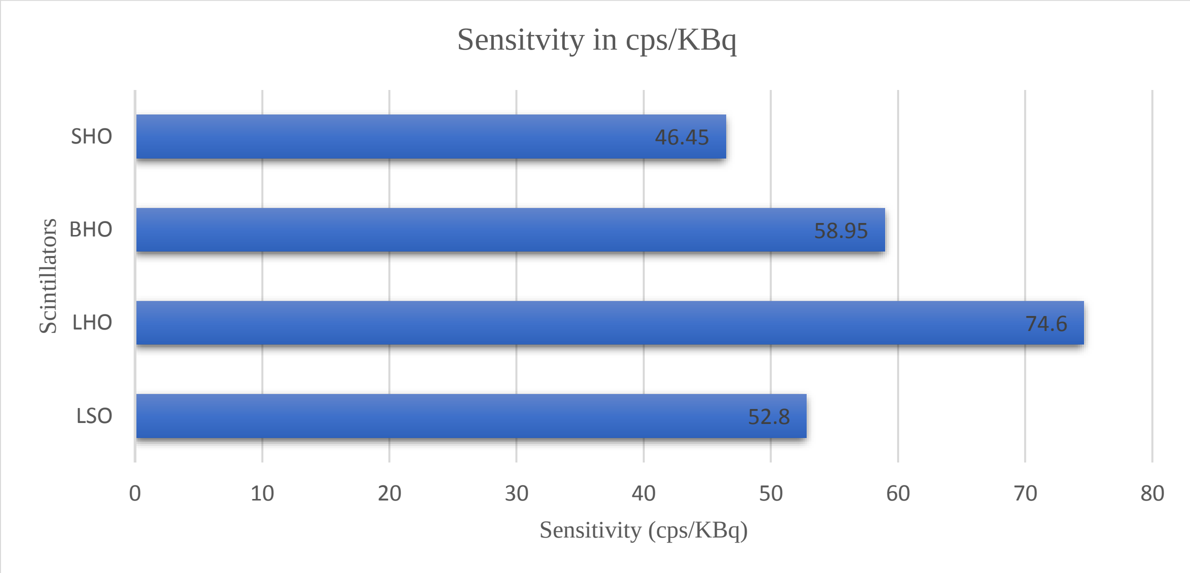

Figure 5.2: Sensitivity in cps/KBq

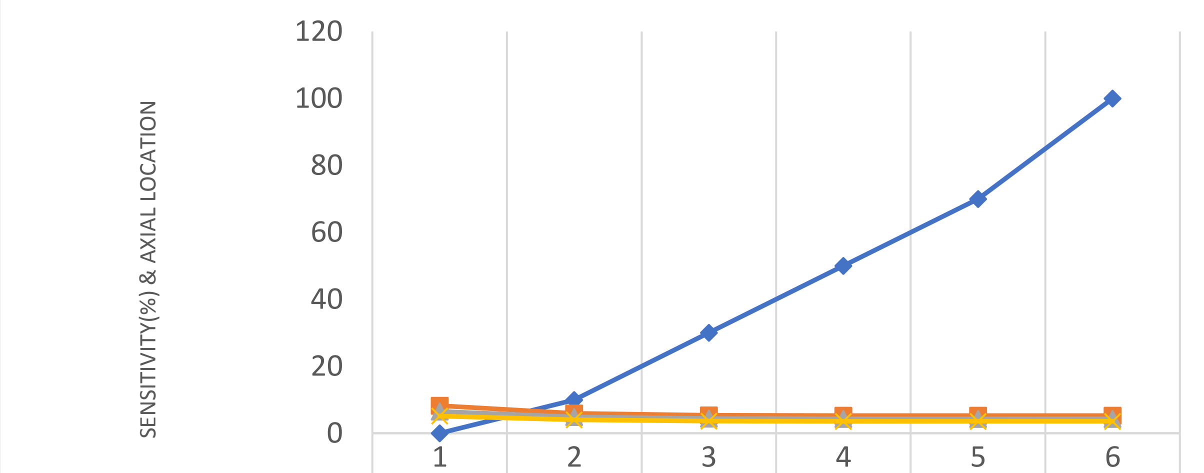

	1	2	3	4	5	6
Axial location	0	10	30	50	70	100
LHO_Sensitivity (%)	8.23	5.93	5.32	5.3	5.27	5.27
BHO_Sensitivity (%)	6.51	4.84	4.38	4.36	4.35	4.33
SHO_Sensitivity (%)	5.13	3.98	3.63	3.59	3.58	3.58

Figure 5. 3: Sensitivity profile across the axial FOV

5.1.2 Spatial resolution

Axial measurement of spatial resolution test result is depicted under Figure 5.4 presents 2D slice of point source image located at CFOV and its mean axial line profile for the suggested found to measure 1.13mm. Table 5.1 shows the achieved spatial resolutions for the suggested scintillators and LSO.

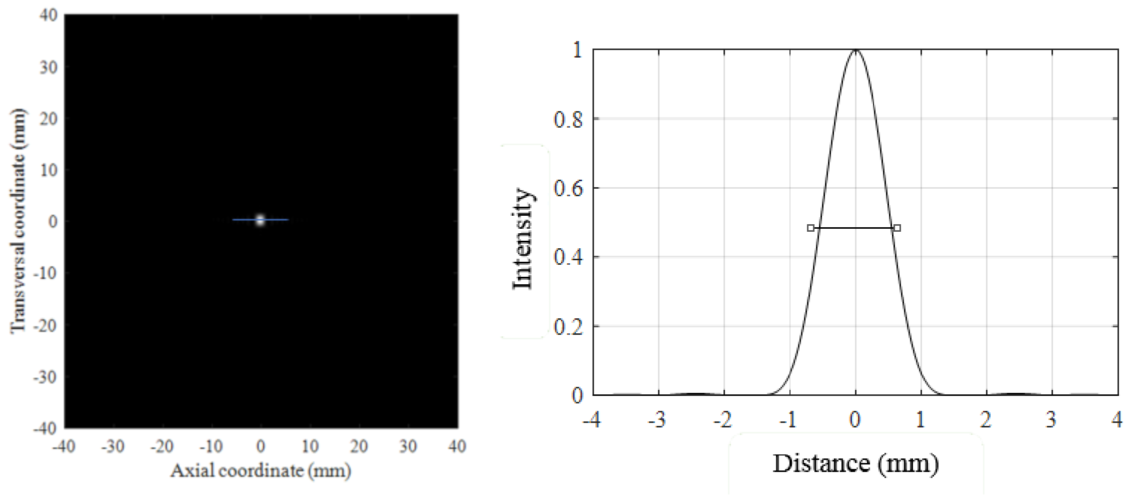

Figure 5.4: Point source image positioned at CFOV (left) and line profile taken axially (right)

Table 5.1: Spatial resolution result

Scintillators	Axial spatial resolution (mm) FWHM
BHO	1.11
LHO	1.10
LSO	1.12
SHO	1.18

5.1.3 Scatter fraction

The mean system scatter fraction is 13.2% and which quiet better than most of scanners comparatively. Figure 5.5 presented the scatter fraction of the system, with different scintillating crystals.

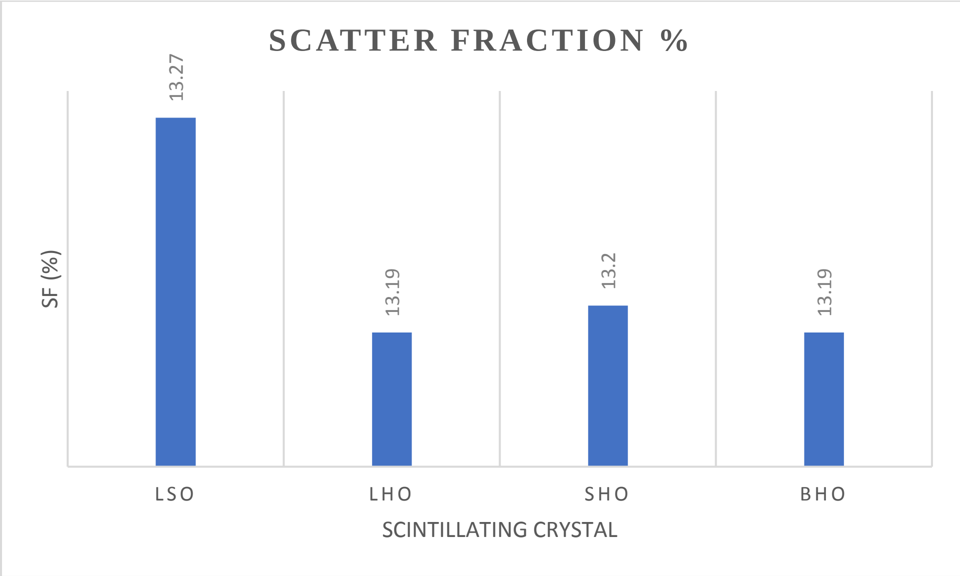

Figure 5. 5: Scatter fraction result of the system tested with different scintillators

5.1.4 Image quality

Figure 5.6A below present's image quality phantom reconstructed image and Figure 5.6B presents the result obtained after processing the simulation coincidence output via direct Fourier transform fully 3D reconstruction algorithm implemented in Matlab.

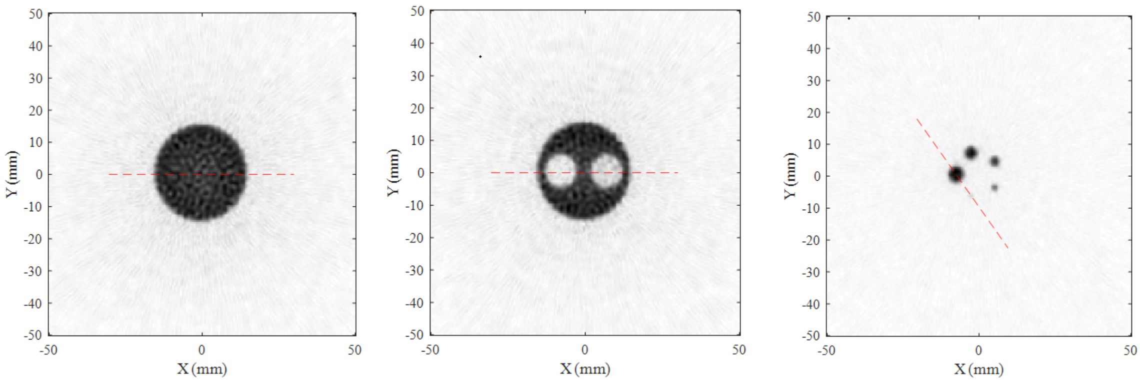

A

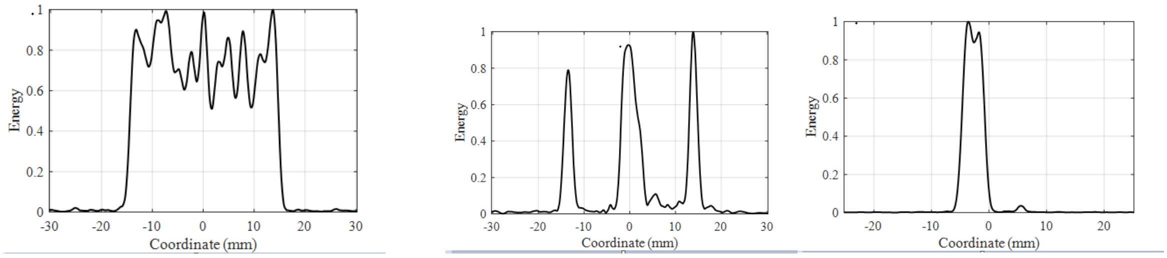

B

Figure 5.6: NEMA image quality phantom a) Image of the NEMA image quality phantom and b) Corresponding line profile.

5.2 Discussion

The spatial resolution test was taken axially and the mean spatial resolution for the suggested scintillators measured at FWHM of the energy found out to be (1.13mm). The measured spatial resolution is found to be promising and even better than commercially available brain PET scanners. Besides, there is no important difference in spatial resolution among three of the scintillator materials employed in the research. This is theoretically proved to be right, according to works of literature the spatial resolution of the system mainly depends on the size of detector (Ri), positron range (Rp), non-collinearity deviation (Ra) and the image reconstruction process (Kr). Since our system with different scintillating materials has the same Ri, Rp, Ra and Kr parameters applying it is not unexpected to have the close spatial resolution for the system since we have collected enough prompt events. The system spatial resolution is presented by in comparison with literature in the field who has implemented the same procedure to test their system performance excluding JPET-D4 system followed a scatter fraction correction procedure.

Table 5. 2: Illustrative comparison of spatial resolution test result for implemented system and existing scanner

Brain PET scanners	Spatial resolution (mm)	References
NEU_PET	Axial=1.13	-------------------
MB-PET	Axial =1.03to 2.05, trans-axial=1.01-1.28	Musa et *al.*, 2018
ECAT HRRT	Axial =<2.4	Jong *et al*., 2007
HRRT-D	Axial=2.5-3.4, trans axial=2.3-3.2	Knoess *et al*., 2002
JPET-D4	Axial =<3	Yoshida *et al*., 2006
WAT-PET	Axial=1.0	Watanabe *et al*., 2017

From the comparison Table (5.2) the achieved resolution level is outstanding and pioneer in the field to implement these materials and present such a valuable result. Furthermore, we are capable to present a novel category of scintillating material with considerable absolute sensitivity ranging from 5.13-8.23% and provided that they have proved as promising scintillators for brain PET imaging. From the comparison plot Figure (5.7) we can see that the suggested material can be implemented in high-performance PET scanner designs.

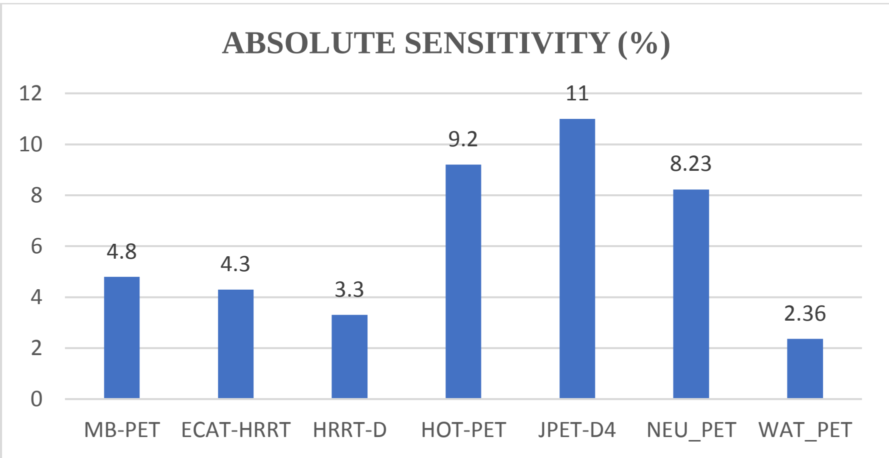

Figure 5.7: Comparative sensitivity presentation of the system

Most of the system mentioned for comparison above has implemented the same procedure and guideline. We presented our system sensitivity represented with the best one 8.23% indicative to be encouraging for high-performance PET scanner implementation. Not only the resolution and sensitivity alone interesting about the result obtained but also the scatter fraction (13.2%) of the system tested following the NEMA NU4-2008 criterion showed to contribute for a good quality image with a stronger SNR. Table 5.3 present comparative description of system scatter fraction. We have presented system scatter fraction comparative to other system implementing the same standard.

Table 5.3: Comparative presentation of system scatter fraction

Brain PET scanners	Scatter fraction %	Energy window Kev
HRRT ECAT PET	52.9	250-650
G-PET	39	410-665
MB-PET	48	350-650
NEU_PET	13.2	350-650

The image quality evaluation of the system revealed systems ability to resolve the 1mm diameter source within the phantom region. From the image quality profiles we can infer that clear and crisp resolution of different sized rods, hot region and cold region and the uniform region with slight spike noise but quite encouraging. The research problem mentioned at the beginning of the study stated that the quest for finding a scintillating crystal with optimum property for PET imaging which should have good light output, shorter decay time, better-stopping power, and emission of visible light that can be addressed by the suggested scintillators. Beyond that demand for having a high-performance brain-specific PET scanner problem can also be addressed via the implemented brain PET system. The Overall results presented in this thesis occupied valuable position comparative to literatures and find out to contribute for the field too.

In the real clinical essence, the results and the study has implication mainly for four things. The first one is to have such high-performance PET can contribute to better cancer diagnosis and mental disorder management. The second one is the study has introduced a new class of scintillating materials for PET application and possibly for other high energy physics studies. Thirdly, since scintillators are cheaper than other detectors we are able to have affordable cost PET scanners to be accessible by the public. Finally, the study has a valuable contribution to the knowledge of the field.

This study has some limitations like any other scientific researches. The study is accomplished using the Monte Carlo algorithm implemented in GATE simulation it has limitation in real-world testing. The test we performed do not cover all procedures mentioned at the NEMANU-4 guideline but approximated to show the applicability of the new class of scintillation material to design a brain PET scanner system.

CHAPTER 6
CONCLUSIONS AND RECOMMENDATIONS

6.1 Conclusions

The purpose of this study was to address the problem related with the demand for high performance brain PET scanner by implementing the TOC scintillators. It majorly aims to design and simulate highly pixelated cerium doped alkaline earth hafnates scintillators based high-performance brain PET scanner using GATE software and evaluate the system performance following NEMA 2008 testing criterion. The study had followed standard PET performance testing developed by NEMA small animal PET testing procedure implementing it through GATE nuclear medicine scanners simulation software.

The results and elaborations presented in this thesis are based on Gate Monte Carlo model for a PET scanner implemented by a newly suggested pixelated scintillating materials LHO, SHO, and BHO. Specific technical PET geometry has been implemented along with the scintillators where the theoretical background obtained from scientific articles. The overall performance test evaluated includes spatial resolution, system scatter fraction, system sensitivity and quality of image test by applying NEMA NU4-2008 standard. The result obtained so far 1.13mm mean axial spatial resolution, 60cps/KBq mean system sensitivity, 13.2% scatter fraction and image quality resolving down to 1 mm rods shows a great promise for high-performance PET scanner design through the suggested scintillators, clinically contributing to play a major role in better diagnosis and mental health problems management. Beyond the mentioned benefits this paper has crucial contribution to the field and able to be used as input for future studies.

6.2 Recommendations

For future studies extended design and techniques can be employed to improve system performance. We also recommend testing the suggested scintillators in real commercial PET scanners with minimal bridging the computer simulation to a real one. Eventually, we call for and encourage implementing the scintillators for other PET geometries.

REFERENCES

Bioimaging. (2014). Presentation. Professor Peyton (2014). Bioimaging PowerPoint (lecture 15). https://openwetware.org/wiki/PET_Imaging_by_Kylee_Klinkowski.

Bailey, D., Maisey, M., Townsend, D., and Valk, P. (2005). Positron Emission Tomography. London: *Springer-Verlag*.

Brain Tumor. (2019). Retrieved from https://www.cancer.net/cancer-types/brain-tumor/statistics.

Budinger, T. (1977). Instrumentation trends in nuclear medicine. *Seminars In Nuclear Medicine*, *7*(4), 285-297. doi: 10.1016/s0001-2998(77)80037-8.

Calderon, Y., Kolstein, M., Uzun, D., De Lorenzo, G., Chmeissani, M., Arce, P., Arino, G., Cabruja, E., Canadas, M., Macias-Montero, J., Martinez, R., Mikhaylova, E., Ozsahin, I. and Puigdengoles, C. (2011). Modeling, simulation, and evaluation of a compton camera based on a pixelated solid-state detector. *2011 IEEE Nuclear Science Symposium Conference Record*.

Cherry, S. (2016). Tomographic Reconstruction in Nuclear Medicine. [online].

Cherry, S.R., and Dahlbom, M. (2004). PET: Physics, Instrumentation and Scanners (pp.1-124). New York, NY: Springer. http://dx.doi.org/10.1007/978-0-387-22529-6_1.

Cherry, S.R., Sorenson, J., and Phelps, M. (2012). *Physics in Nuclear Medicine*. Philadelphia, Pa: Saunders.

E. Rutherford, J. Chadwich, C.D. Ellis. (1930) Radiations from Radioactive Substances, *Cambridge University Press*, Cambridge.

Flickr (2006). Pair production. Retrieved December 13, 2018 from https://www.flickr.com/photos/mitopencourseware/4706123553.

Freifelder, R., Karp, J., Geagan, M., & Muehllehner, G. (1994). Design and performance of the HEAD PENN-PET scanner. *IEEE Transactions On Nuclear Science*, *41*(4), 1436-1440. doi: 10.1109/23.322928.

GATE: A simulation toolkit for PET and SPECT. *Physics in Medicine and Biology*, 49, 4543-4561

GATE collaboration (2016). Users Guide V7.2. *http://wiki.opengatecollaboration.org/index.php/Users_Guide_V7.2*.

G.F. Knoll. (1999). Radiation Detection and Measurement - 3rd edition (Chapters 16 to 18), John Wiley & Sons.

G.F. Knoll. (2000) Radiation Detection and Measurement, 3rd Edition, Wiley, New York.

Gong, K., Majewski, S., Kinahan, P., Harrison, R., Elston, B., & Manjeshwar, R. et al. (2016). Designing a compact high performance brain PET scanner—simulation study. *Physics In Medicine And Biology*, *61*(10), 3681-3697. doi: 10.1088/0031-9155/61/10/3681.

Herbert, D., Moehrs, S., D'Ascenzo, N., Belcari, N., Del Guerra, A., Morsani, F., & Saveliev, V. (2007). The Silicon Photomultiplier for application to high-resolution Positron Emission Tomography. Nuclear Instruments and Methods In Physics Research Section A: Accelerators, Spectrometers, Detectors And Associated Equipment, 573(1-2), 84-87. doi: 10.1016/j.nima.2006.11.020.

Hofstadter, R. (1948). Alkali Halide Scintillation Counters. *Physical Review*, 74(1), 100-101. doi: 10.1103/physrev.74.100.

H. Fahey, F. (2002). Data Acquisition in PET Imaging. *Journal Of Nuclear Medicine*, *30*(2), 39-49. Retrieved from http://tech.snmjournals.org/content/30/2/39.fullFrederic.

Imagingkt (2016). Physical Interaction processes. Retrieved December 13, 2018 from http://199.116.233.101/index.php/Physical_Interaction_processes. *International Workshop on Bismuth Germanate. (1982),* Princeton University, Princeton.

Jan, S., Santin, G., Strul, D., Staelens, S., Assié, K., Autret, D. Morel, C. (2004).

Jie Zheng. (2012). Energy metabolism of cancer: Glycolysis versus oxidative phosphorylation (Review). *Oncology letters*. *4(6):* 1151–1157. doi: 10.3892/ol.2012.928.

Jong, H., Velden, F., Kloet, R., Buijs, F., Boellaard, R. and Lammertsma, A. (2007). Performance evaluation of the ECAT HRRT: an LSO-LYSO double layer high resolution, high sensitivity scanner. *Physics in Medicine and Biology*, 52(5), pp.1505-1526.

K.A Johnson, et al. (2015) Imaging in aging and early Alzheimer disease. *Ann. Neurol*. 79(1),pp.110-119.

Knoess, C., Boellaard, R., Lenox, M., Vollmar, S., Casey, M., Fluegge, G., Lammertsma, A., Wienhard, K. and Heiss, W. (2002). Evaluation of the depth of interaction (DOI) for the High

Resolution Research Tomograph (HRRT) - a comparison between scanners with and without DOI. *2002 IEEE Nuclear Science Symposium Conference Record*.

Kolstein, M., Lorenzo, G., Mikhaylova, E., Chmeissani, M., Ariño, G., & Calderón, Y. et al. (2013). Evaluation of Origin Ensemble algorithm for image reconstruction for pixelated solid-state detectors with large number of channels. *Journal Of Instrumentation*, *8*(04), P04030-P04030. doi: 10.1088/1748-0221/8/04/p04030 .

Lecoq, P (2016). Development of new scintillators for medical applications. Nuclear and methods in physics research section A: Accelerators, spectrometers, Detectors and Associated Equipment 809, pp. 130-139.

Lempicki, A., Wojtowicz, A., & Berman, E. (1993). Fundamental limits of scintillator performance. *Nuclear Instruments And Methods In Physics Research Section A: Accelerators, Spectrometers, Detectors And Associated Equipment*, *333*(2-3), 304-311. doi: 10.1016/0168-9002(93)91170-r .

L. Melcher, C. (2000). Scintillation Crystals for PET. *Journal Of Nuclear Medicine*, 41, 1051-1055.

Marcus, C., Mena, E., & Subramaniam, R. (2014). Brain PET in the Diagnosis of Alzheimer's disease. *Clinical Nuclear Medicine*, 39(10), e413-e426. doi: 10.1097/rlu.0000000000000547.

Mendes, P., Bruyndonckx, P., Castro, M., Li, Z., Perez, J., & Martin, I. (2008). Optimization of a monolithic detector block design for a prototype human brain PET scanner. *2008 IEEE Nuclear Science Symposium Conference Record*. doi: 10.1109/nssmic.2008.4774345.

Mikhaylova, E., De Lorenzo, G., Chmeissani, M., Kolstein, M., Canadas, M., & Arce, P. et al. (2014). Simulation of the Expected Performance of a Seamless Scanner for Brain PET Based on Highly Pixelated CdTe Detectors. *IEEE Transactions On Medical Imaging*, *33*(2), 332-339. doi: 10.1109/tmi.2013.2284657 .

Miller et. al. (2008). Angewandte Chem. Int. Ed. 47, 8998-9033. Retrieved from https://www.triumf.ca/radiochemistry-for-pet-imaging .

Morimoto, Y., Ueno, Y., Takeuchi, W., Kojima, S., Matsuzaki, K., Ishitsu, T., Umegaki, K., Kiyanagi, Y., Kubo, N., Katoh, C., Shiga, T., Shirato, H. and Tamaki, N. (2011). Development of a 3D Brain PET Scanner Using CdTe Semiconductor Detectors and Its First Clinical Application. *IEEE Transactions on Nuclear Science*, 58(5), pp.2181-2189.

Musa, m., Ozsahin, D. and Ozsahin, I. (2017). Simulation and evaluation of a cost-effective high-performance brain PET scanner. *J Biomed Imag Bioeng*, [online] 1(2), pp.53-59. Available at: http://www.alliedacademies.org/articles/simulation-and-evaluation-of-a-costeffective-highperformance-brain-pet-scanner-8916.html [Accessed 18 Feb. 2018].

Musa, M., Ozsahin, D. and Ozsahin, I. (2018). Simulation and evaluation of high-performance cost-effective positron emission mammography scanner. *Journal of Instrumentation*, 13(11), pp.C11023-C11023.

M. Levy, Fortschr. Geb. Rontgenstr.(1897) 1(75).

Nagy, K., Toth, M., Major, P., Patay, G., Egri, G., & Haggkvist, J. et al. (2013). Performance Evaluation of the Small-Animal nanoScan PET/MRI System. *Journal Of Nuclear Medicine*, *54*(10), 1825-1832. doi: 10.2967/jnumed.112.119065.

Nassalski, A., Kapusta, M., Batsch, T., Wolski, D., Mockel, D., Enghardt, W., & Moszynski, M. (2007). Comparative Study of Scintillators for PET/CT Detectors. *IEEE Transactions On Nuclear Science*, 54(1), 3-10. doi: 10.1109/tns.2006.890013.

NEMA Standards Publication NU 4 – 2008 Performance Measurements of Small Animal Positron Emission Tomographs. (2008). *National Electrical Manufacturers Association.* www.nema.org

Ozsahin, I. and Unlu, M. (2014). Modeling and simulation of Positron Emission Mammography (PEM) based on double-sided CdTe strip detectors. *Journal of Instrumentation*, 9(03), pp.C03055-C03055.

Ozsahin, D., Bläckberg, L., Fakhri, G. and Sabet, H. (2017). GATE simulation of a new design of pinhole SPECT system for small animal brain imaging. Journal of Instrumentation, 12(01), pp.C01085-C01085.

Ozsahin, D., Uzun, B., Musa, M., Şentürk, N., Nurçin, F. and Ozsahin, I. (2017). Evaluating nuclear medicine imaging devices using fuzzy PROMETHEE method. Procedia Computer Science, 120, pp.699-705.

Ozsahin, D., Isa, N., Uzun, B. and Ozsahin, I. (2018). Effective analysis of image reconstruction algorithms in nuclear medicine using fuzzy PROMETHEE. 2018 Advances in Science and Engineering Technology International Conferences (ASET).

Ozsahin, I., Sharif, T., Ozsahin, D. and Uzun, B. (2019). Evaluation of solid-state detectors in medical imaging with fuzzy PROMETHEE. *Journal of Instrumentation*, 14(01), pp.C01019-C01019.

PET plus CT. (2018). Retrieved from https://www.mayoclinic.org/tests-procedures/pet-scan/multimedia/pet-plus-ct/img-20005900.

Pizzichemi, M. (2016). Positron Emission Tomography: state of the art and future developments. *Journal Of Instrumentation*, *11*(08), C08004-C08004. doi: 10.1088/1748-0221/11/08/c08004.

Portnow, L., Vaillancourt, D., & Okun, M. (2013). The history of cerebral PET scanning: From physiology to cutting-edge technology. *Neurology*, *80*(10), 952-956. doi: 10.1212/wnl.0b013e318285c135.

Radiology Key. Available at: https://radiologykey.com/tomographic-reconstruction-in-nuclear-medicine/ [Accessed 4 Apr. 2019].

Rahmim, A. (2006). PET vs. SPECT: in the Context of Ongoing Developments (Review Article). Iran J Nucl Med, 14(25). R. Hofstadter. (1975*). IEEE Trans. Nucl. Sci*. NS-22, 13.

Schlemmer, H., Pichler, B., Schmand, M., Burbar, Z., Michel, C., & Ladebeck, R. et al. (2008). Simultaneous MR/PET Imaging of the Human Brain: Feasibility Study. *Radiology*, *248*(3), 1028-1035. doi: 10.1148/radiol.2483071927.

Séguinot, Jacques ; Braem, André ; Chesi, Enrico Guido ; Joram, C ; Mathot, S ; Weilhammer, P ; Chamizo-Llatas, M ; Correia, J G ; Ribeiro da Silva, M ; Garibaldi, F ; De Leo, R ; Nappi, E ; Corsi, F ; Dragone, A ; Schoenahl, F ; Zaidi, H. . (2004). Novel Geometrical Concept of a High Performance Brain PET Scanner: Principle, Design and Performance Estimates. Nuovo Cimento C, [online] 029 (2006) 429-463(029 (2006), pp.429-463. Available at: http://cds.cern.ch/record/796104# [Accessed 5 May 2019].

Shi, H., Du, D., Xu, J., Su, Z., & Peng, Q. (2015). Design study of dedicated brain PET with polyhedron geometry. *Technology And Health Care*, *23*(s2), S615-S623. doi: 10.3233/thc-151000.

Shiga, T., Morimoto, Y., Kubo, N., Katoh, N., Katoh, C., & Takeuchi, W. et al. (2008). A New PET Scanner with Semiconductor Detectors Enables Better Identification of Intratumoral

Inhomogeneity. *Journal Of Nuclear Medicine*, *50*(1), 148-155. doi: 10.2967/jnumed.108.054833.

şın, A., Ozsahin, D., Dutta, J., Haddani, S. and El-Fakhri, G. (2017). Monte Carlo simulation of PET/MR scanner and assessment of motion correction strategies. Journal of Instrumentation, 12(03), pp.C03089-C03089.

S. Karp, J., Surti, S., E., M., Witherspoon, D., Freifelder, R., & A. Cardi, C. et al. (2003). Performance of a Brain PET Camera Based on Anger-Logic Gadolinium Oxyorthosilicate Detectors. *J Nucl Med*, *44*, 1340–1349.

Spiedigitallibrary.org. (2019) search the world's largest collection of optics and photonics applied research. [Online] Available at: https://www.spiedigitallibrary.org [accessed 5 May 2019].

Staelens, S., Strul, D., Santin, G., Vandenberghe, S., Koole, M., & D Asseler, Y. et al. (2003). Monte Carlo simulations of a scintillation camera using GATE: validation and application modelling. *Physics In Medicine And Biology*, *48*(18), 3021-3042. doi: 10.1088/0031-9155/48/18/305.

Stanford: Advanced Optical Ceramics Laboratory. (2018). Retrieved from https://web.stanford.edu/group/scintillators/scintillators.html .

Stephen E Derenzo, WW Moses, JL Cahoon, RCC Perera, JE Litton. (1990). Prospects of new inorganic scintillators. *IEEE transactions on nuclear science.* 37(2),203-208.

Sweet, W. (1951). The Uses of Nuclear Disintegration in the Diagnosis and Treatment of Brain Tumor. *New England Journal Of Medicine*, 245(23), 875-878. doi: 10.1056/nejm195112062452301.

Surti, S. (2014). Update on Time-of-Flight PET Imaging. *Journal Of Nuclear Medicine*, *56*(1), 98-105. doi: 10.2967/jnumed.114.145029.

Surti, S., & Karp, J. (2016). Advances in time-of-flight PET. *Physica Medica*, *32*(1), 12-22. doi: 10.1016/j.ejmp.2015.12.007.

T.A. Edison, (1896). Nature 470.

Terry Jones and David Townsend. (2017). History and future technical innovation in positron emission tomography. J. Med. Imag. 4(1), 011013. doi: 10.1117/1.JMI.4.1.011013.Vandenberghe, S., Mikhaylova, E., D'Hoe, E., Mollet, P., & Karp,

J. (2016). Recent developments in time-of-flight PET. *EJNMMI Physics*, 3(1). doi: 10.1186/s40658-016-0138-3.

Tong, S., Alessio, A., & Kinahan, P. (2010). Image reconstruction for PET/CT scanners: past achievements and future challenges. *Imaging In Medicine, 2*(5), 529-545. doi: 10.2217/iim.10.49.

Tohme, M., & Qi, J. (2009). Iterative image reconstruction for positron emission tomography based on a detector response function estimated from point source measurements. *Physics In Medicine And Biology*, *54*(12), 3709-3725. doi: 10.1088/0031-9155/54/12/007.

Uzun, D., Lorenzo, G., Kolstein, M. and Chmeissani, M. (2014). Simulation and evaluation of a high resolution VIP PEM system with a dedicated LM-OSEM algorithm. *Journal of Instrumentation*, 9(05), pp.C05011-C05011.

Uzun-Ozsahin, D., Blackberg, L., Moghadam, N., Fakhri, G. and Sabet, H. (2016). GATE simulation of a high-performance stationary SPECT system for cardiac imaging. *2016 IEEE Nuclear Science Symposium, Medical Imaging Conference and Room-Temperature Semiconductor Detector Workshop (NSS/MIC/RTSD).*

Vandenbroucke, A., Foudray, A., Olcott, P. and Levin, C. (2010). Performance characterization of a new high resolution PET scintillation detector. *Physics in Medicine and Biology*, 55(19), pp.5895-5911.

Van Loef, E., Higgins, W., Glodo, J., Brecher, C., Lempicki, A., & Venkataramani, V. et al. (2007). Scintillation Properties of SrHfO3:Ce3+ and BaHfO3:Ce 3+ Ceramics. *IEEE Transactions On Nuclear Science,* 54(3), 741-743. doi: 10.1109/tns.2007.896343.

Valk, P. (2006). *Positron emission tomography*. London: Springer.

Vaquero, J. and Kinahan, P. (2015). Positron Emission Tomography: Current Challenges and Opportunities for Technological Advances in Clinical and Preclinical Imaging Systems. *Annual Review of Biomedical Engineering*, 17(1), pp.385-414.

Venkataramani V.S, Loureiro S.M, Rane V. (2003). Cerium-doped alkaline-earth Hafnium oxide scintillators having Improved transparency and Method of making the same. *United States Patent Application Publication.* Pub. No.: US 2003/0193040 A1.

Watanabe, M., Shimizu, K., Omura, T., Takahashi, M., Kosugi, T., & Yoshikawa, E. et al. (2002). A new high-resolution PET scanner dedicated to brain research. *IEEE Transactions On Nuclear Science*, 49(3), 634-639. doi: 10.1109/tns.2002.1039541.

Watanabe, M., Saito, A., Isobe, T., Ote, K., Yamada, R., Moriya, T. and Omura, T. (2017). Performance evaluation of a high-resolution brain PET scanner using four-layer MPPC DOI detectors. *Physics in Medicine & Biology*, 62(17), pp.7148-7166.

Weber, M.J. (2002). Inorganic scintillators: today and tomorrow. *Journal Of Luminescence*, *100*(1-4), 35-45. doi: 10.1016/s0022-2313(02)00423-4.

Wienhard, K., Schmand, M., Casey, M., Baker, K., Bao, J., & Eriksson, L. et al. (2002). The ECAT HRRT: performance and first clinical application of the new high resolution research tomograph. *IEEE Transactions On Nuclear Science*, *49*(1), 104-110. doi: 10.1109/tns.2002.998689.

Yoshida, E., Kobayashi, A., Yamaya, T., Watanabe, M., Nishikido, F., Kitamura, K., Hasegawa, T., Fukushi, M. and Murayama, H. (2006). The JPET-D4: Performance evaluation of four-layer DOI-PET scanner using the NEMA NU2-2001 standard. *IEEE Nuclear Science Symposium Conference Record*.

Zhang, J., Maniawski, P., & Knopp, M. (2018). Performance evaluation of the next generation solid-state digital photon counting PET/CT system. *EJNMMI Research*, *8*(1). doi: 10.1186/s13550-018-0448-7.